This is a non-peer-reviewed preprint submitted to EarthArXiv.

Extensive Olivine Depletion in Archean Greenstone Belts: Evidence from Drill Core and Implications for Natural Hydrogen Generation

Jiejie Li[1*], Peter W Haines[2], Andrew Feitz[3], T David Waite[1] and Ryan T Armstrong[1]

[1]School of Civil and Environmental Engineering, UNSW Sydney, Sydney, Australia
[2]Geological Survey of Western Australia, Perth, Australia
[3]Geoscience Australia, Canberra, Australia

Author email addresses

Jiejie Li: jiejie.li@unsw.edu.au; drjiejielee@gmail.com
Peter W Haines: peter.haines@dmpe.wa.gov.au
Andrew Feitz: andrew.feitz@ga.gov.au
T David Waite: d.waite@unsw.edu.au
Ryan T Armstrong: ryan.armstrong@unsw.edu.au

***Corresponding author:** Jiejie Li (jiejie.li@unsw.edu.au; drjiejielee@gmail.com)

Peer-review status: This manuscript is a preprint and has not been peer reviewed. Subsequent versions of this manuscript may have slightly different content.

Extensive Olivine Depletion in Archean Greenstone Belts: Evidence from Drill Core and Implications for Natural Hydrogen Generation

Jiejie Li[1], Peter W Haines[2], Andrew Feitz[3], T David Waite[1] and Ryan T Armstrong[1]

1. *School of Civil and Environmental Engineering, UNSW Sydney, Sydney, Australia.*
2. *Geological Survey of Western Australia, Perth, Australia.*
3. *Geoscience Australia, Canberra, Australia.*

Abstract

Natural hydrogen models commonly assume that ultramafic rocks in Archean greenstone belts retain olivine for continued serpentinization, but the regional extent of preservation is poorly constrained. We analyze thermal-infrared mineral logs from 18,692 m of ultramafic drill core in 218 Western Australian boreholes. Olivine exceeds a defined spectral threshold in 97% of intrusion-hosted core but only 24% of greenstone-hosted core, a contrast robust to threshold selection and borehole or cluster weighting. Talc–carbonate assemblages dominate 56% of greenstone-hosted core. Fewer than 1% of these intervals meet the olivine criterion. Mineral assemblages are spatially clustered even within tectonic units (permutation $p \leq 0.007$), and serpentine declines relative to olivine below 100 m. These results reveal extensive but spatially uneven olivine depletion in the sampled Archean greenstones, challenging the premise of broadly retained olivine in greenstone-based natural hydrogen source models. Assessing remaining olivine therefore requires mineralogical evidence rather than lithological extent alone.

Main Contributions

- Thermal-infrared logs detect olivine in 24% of greenstone-hosted ultramafic core in Western Australia, against 97% in ultramafic intrusions
- Over half of greenstone-hosted core is talc–carbonate-dominated, and less than 1% of this core meets the olivine criterion
- Neighboring boreholes share mineral state within tectonic units, so olivine-based source assessments need local mineralogical data

1. Introduction

Serpentinization hydrates olivine-rich rock and oxidizes its ferrous iron, releasing hydrogen (Evans et al., 2013; Klein et al., 2009; Sleep et al., 2004; Tutolo & Tosca, 2023). The yield depends on temperature, on iron partitioning among the products, and on the protolith (Klein et al., 2013; McCollom & Bach, 2009). Assessments of natural hydrogen as a resource (Zgonnik, 2020) address two questions at different scales: (1) how much hydrogen exists globally, and (2) where within a particular region it can be generated. The global question has been addressed using a mass-balance model (Ellis & Gelman, 2024), but the model does not predict where hydrogen generation occurs. The regional question, which guides exploration, depends on where rock capable of generating hydrogen is present.

At this regional scale, Archean greenstone belts are listed among terranes that are prospective for hydrogen generation by water–rock reaction (Ballentine et al., 2025), consistent with a substantial Precambrian contribution to global hydrogen production (Sherwood Lollar et al., 2014). The Cratonic Greenstone Model assumes that greenstone-belt ultramafic rocks, although partly serpentinized, retain sufficient remnant olivine for further serpentinization “in most cases” (Hutchinson et al., 2024). Play-based exploration models and case studies for cratonic settings likewise take

ultramafic basement rock as a source (Donzé et al., 2020; Jackson et al., 2024). Ballentine et al. (2025) calculate reference yields for unreacted ultramafic rock, identify the mineralogy and amount of reacted rock as critical uncertainties, and highlight improved estimation of hydrogen generation by water–rock reaction as a research priority. Exploration workflows, accordingly, call for measurement of the remaining Fe(II) content of a rock and its heterogeneity within a formation (Lévy et al., 2023), because olivine no longer generates hydrogen once altered (Etiope et al., 2026). Recent generation models distinguish remaining reactive rock from total rock volume (Christiansen et al., 2026) and treat mineralogical characterization as central to assessing generation potential (Andreani et al., 2013; Geymond et al., 2025; Li et al., 2026a).

However, alteration does not always leave olivine behind, and in greenstone belts olivine retention has been documented only at individual deposits. Alteration can remove olivine or create it. For example, carbonation can result in the complete replacement of Mg-silicates (Beinlich et al., 2012; Falk & Kelemen, 2015; Menzel et al., 2022), successive serpentinization, carbonation, and silica metasomatism can occur (Schwarzenbach et al., 2021), and olivine can be formed during prograde metamorphism (Ulrich et al., 2024). Within single bodies, komatiite-hosted nickel deposits show serpentinite or olivine-bearing cores and talc–carbonate margins (Caruso et al., 2020; Gole et al., 1987; Hill et al., 2004) and dunite on the lower-grade side of the olivine isograd is serpentinized (Gole, 2014; Grguric et al., 2006). Alteration also changes with depth. For example, in drilled ophiolitic peridotite in Oman, the upper 100–250 m is fully serpentinized while the underlying section is only partly serpentinized (Kelemen et al., 2021; Templeton et al., 2024). It is clear from the literature that a systematic regional measure is lacking, both of how commonly greenstone-hosted ultramafic rock still contains olivine and of the scale at which olivine content varies.

Herein, using the drilled mineralogical record of Western Australia, we examine the extent to which greenstone-hosted ultramafic rock still contains olivine and identify the scale at which its occurrence varies. The unresolved question is not whether ultramafic rocks undergo alteration, but whether olivine retention is sufficiently widespread to support the premise that reactive source rocks may remain in Archean greenstone belts. The Yilgarn Craton suits this analysis. Its komatiite-hosted nickel deposits, the largest Archean nickel endowment in Australia, have been extensively drilled (Barnes & Fiorentini, 2012; Mole et al., 2014), and the region is considered prospective for natural hydrogen (Rezaee, 2021), with hydrogen already reported in shallow wells and surface seeps (Boreham et al., 2021; Davies et al., 2024). Coupled hydrogen production and carbon mineralization (Osselin et al., 2022) has already been modeled there (Zeng et al., 2026). The Geological Survey of Western Australia provides thermal-infrared logs of selected drill core held within its core libraries, which record anhydrous silicates such as olivine (Schodlok, Whitbourn, et al., 2016). Earlier regional uses of HyLogger data mapped alteration mineralogy (Huntington et al., 2006) or predicted geochemistry (Kutzke et al., 2022). We compile a per-meter inventory of 18,692 m of ultramafic core from 218 boreholes and test whether (1) olivine is common in greenstone-hosted core, (2) the mineral state is coherent at the scale of local borehole clusters within tectonic units, and (3) olivine content relative to serpentine changes with depth below the weathering zone.

2. Data and Methods

2.1 Hyperspectral drill-core archive and per-meter mineralogy

The National Virtual Core Library (NVCL) holds continuous HyLogger reflectance scans of drill core in the visible–near-infrared, shortwave-infrared (SWIR), and thermal-infrared (TIR) ranges (Laukamp et al., 2026; Schodlok, Whitbourn, et al., 2016). Screening every dataset with a usable TIR log (5,100 datasets, accessed September 5, 2026) identified 603 cores with an ultramafic signature. Of the 34 cores in which at least 5% of the valid TIR spectra are classified as olivine, 33 are in Western Australia (**Section S1**, **Table S1**). We use the 359 Western Australian candidate records and Geological Survey of Western Australia (GSWA) Summary Mineral Logs, which report the weight of each

mineral group from TIR (jCLST) and SWIR (TSA+) unmixing at 1 m intervals (**Section S2**). The TIR weights come from spectral unmixing, which fits each measured spectrum as a weighted combination of reference mineral spectra from a library (Schodlok, Green, & Huntington, 2016; Green et al., 2026; Laukamp et al., 2021). Published validation covers only visible to shortwave-infrared estimates in an iron ore deposit (Haest et al., 2012) and the joint unmixing algorithm on analyzed reference samples (Green et al., 2026). To our knowledge, the TIR weights have not been calibrated against quantitative mineralogy in komatiite or cumulate rock. We therefore use them as relative spectral proportions, to rank each 1 m interval and to flag whether a mineral group meets a stated criterion.

A 1 m interval is deemed ultramafic where serpentine (Srp) + olivine (Ol) + talc (Tlc) + carbonate (Cb) $\geq$ 0.5, and Srp + Ol + Tlc $\geq$ 0.3, which excludes carbonate-dominated (quartz–carbonate) intervals. Tlc is the log's Other-MgOH group, dominated by talc in the TIR. Pyroxene, amphibole, and chlorite are reported as separate groups and are not counted in the criterion, because they are also major phases of mafic rock (Section S2). Requiring the olivine weight to exceed the pyroxene weight changes the olivine-bearing share of each host category by at most one percentage point. The archive contains 18,692 such 1 m intervals (hereafter meters) in 219 records (HyLogger datasets) from 218 boreholes, one of which has two records. Each meter is described by two assemblage indices: X_{hyd} = Srp/(Srp + Ol), the serpentine share of the olivine–serpentine pair, and X_{carb} = (Tlc + Cb)/(Srp + Ol + Tlc + Cb), the talc-plus-carbonate share of the four groups. X_{hyd} is defined only where Srp + Ol $\geq$ 0.1, twice the minimum bin weight of the unmixing. Meter intervals with $X_{hyd} < 0.2$ are termed olivine-dominated, those with $X_{hyd} > 0.8$ are serpentine-dominated, and those with $X_{carb} > 0.8$ are deemed talc–carbonate-dominated. Olivine-bearing meters have an unmixing weight Ol > 0.05, and meters with SWIR smectite + kaolin > 0.2 are clay-rich. In 4,856 quartz-rich and 30,139 quartz-bearing felsic meters of the same logs, selected without reference to the olivine weight, Ol never exceeds 0.05 (Section S5). This describes the spectral background of the olivine weight, not an independent validation. Confirming the olivine criterion, including whether olivine is missed in talc–carbonate-rich mixtures, requires quantitative mineralogy of representative core, such as XRD with Rietveld refinement or thin-section point counts, which is beyond the scope of this archive-based study. The reported olivine-bearing fractions are therefore proportions of core meeting the spectral criterion, not of core containing olivine, which may lie below the detection threshold or be unresolved in strongly altered assemblages. Across the tested ranges of the ultramafic criterion (0.4–0.6), the X_{hyd} denominator threshold (0.02–0.30), and the class cut-offs (0.1/0.9 to 0.3/0.7), the olivine-dominated fraction varies only between 0.28 and 0.36 and its depth pattern is unchanged (**Section S2.3**, **Tables S2–S4**).

2.2 Tectonic units, host units and borehole clusters

Each borehole was assigned by collar position to a tectonic unit of the GSWA 1:10 000 000 tectonic map (Department of Energy, Mines, Industry Regulation and Safety [DEMIRS], 2023) and to a mapped host unit, the bedrock unit at the collar in the GSWA 1:500 000 interpreted bedrock geology (DEMIRS, 2018; Section S3). Because boreholes in a prospect commonly intersect the same body, boreholes with ultramafic core are grouped into clusters in which each lies within 5 km (the linking distance) of another. The 218 boreholes form 110 clusters, and their number changes little with the linking distance (**Section S3**). Each cluster is assigned to the host unit holding most of its ultramafic meters, and host units are grouped by name into three mapped host categories: layered intrusions or cumulates (six named units), greenstone belts (names containing "greenstone"), and other mapped hosts (**Table S5**). These categories describe map polygons at the collar, not the rock logged at depth. Depths are along-hole, because the mineral logs do not record inclination.

2.3 Statistical analysis

Depth profiles of the clay-rich share and of X_{hyd} are per-borehole means within depth intervals, averaged over boreholes. The surface clay zone of a borehole is defined in **Section S2.4**.

Within-borehole trends use the meters below 100 m in the 34 boreholes with at least 30 defined X_{hyd} meters spanning at least 200 m. Each borehole slope is the least-squares slope of X_{hyd} on depth, with a 95% interval from a moving-block bootstrap of 10 m blocks. The pooled slope of a group is the common slope after removing borehole means, with a 95% interval from resampling whole boreholes (**Section S4.1**). Pooled X_{carb} slopes use every ultramafic meter below 100 m of the same boreholes.

The mineral state of a cluster is the share of olivine, serpentine, and talc + carbonate in the summed TIR weights of its ultramafic meters, for the 65 clusters with at least 50 such meters (**Figure 3**). Whether boreholes of the same cluster are more alike than their tectonic unit implies is tested by permuting cluster labels among the boreholes of each unit (**Section S4.3**). Olivine-bearing shares of the host categories are weighted per meter, per borehole, and per cluster, with 95% intervals from resampling whole clusters within each category (**Section S5**).

3. Results

3.1 Olivine occurrence by mapped host category

The ultramafic criterion selects 219 of the 359 candidate records, from 218 of the 1,897 NVCL boreholes in Western Australia, of which 139 hold ≥ 30 m of ultramafic core (**Figure 1a**). Most of this core lies in the greenstone belts of the Yilgarn Craton, three quarters of it in the Eastern Goldfields Superterrane and Youanmi Terrane (**Figure 1c**), and two thirds lies more than 200 m below the collar (**Figure 1b)** and below the weathering zone (**Section 3.2**). The archive therefore mainly samples the setting that regional source models target.

Olivine meets the criterion (Ol > 0.05) in 32% of the ultramafic meters, but this share separates the mapped host categories: 97% (95% interval 87–100%) in the layered intrusions against 24% (10–35%) in the greenstone belts (**Figure 1d**; Table S6a). The contrast persists when each borehole (98% against 12%) or each cluster (97% against 18%) is weighted equally and for olivine thresholds from 0.02 to 0.15 (88–99% against 20–26%). Only 17% of greenstone-belt boreholes hold ≥ 10 m of olivine-bearing core (**Section S5**, **Table S8**). Leaving out any one cluster or the longest borehole keeps the greenstone-belt share at 17–26%, and excluding the Eastern Goldfields Superterrane raises it to 38%. By tectonic unit, nearly all of the core in the Musgrave Province and Halls Creek Orogen is olivine-bearing, against 18% in the Eastern Goldfields Superterrane, where serpentine and talc–carbonate dominate (**Figure 1c**). Talc–carbonate-dominated meters form 49% of all ultramafic core and 56% of the greenstone-belt category, and fewer than 1% of them meet the olivine criterion. Olivine-dominated meters make up about a third of those with X_{hyd} defined and are concentrated in 29 boreholes (ringed in **Figure 1a**).

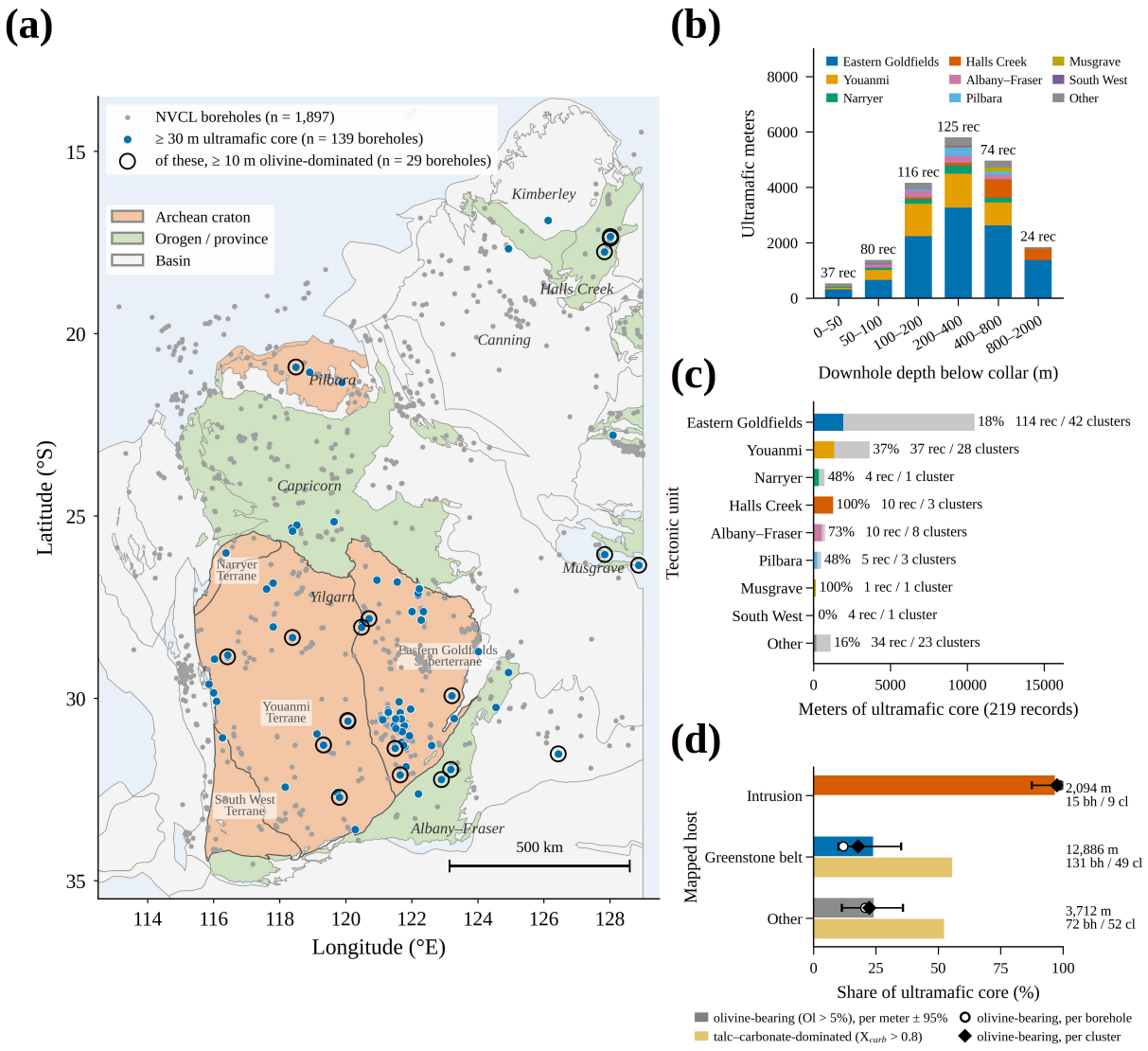


Figure 1. The hyperspectral drill core archive of ultramafic rock in Western Australia. (a) All 1,897 NVCL boreholes (grey) on GSWA 1:10 M tectonic units. Blue symbols mark the 139 boreholes with ≥ 30 m of ultramafic core, and black rings the 29 with ≥ 10 m of olivine-dominated meters (X_{hyd} < 0.2). (b) Ultramafic meters by downhole depth, stacked by tectonic unit, with the number of records per interval. (c) Ultramafic meters (grey) and olivine-bearing meters (Ol > 0.05, colored) by tectonic unit, with the olivine-bearing percentage and the numbers of records and 5 km clusters. (d) Olivine-bearing share of ultramafic core by mapped host category, per meter (bars, 95% intervals from resampling clusters), per borehole (open circles), and per cluster (diamonds), with the talc–carbonate-dominated share (X_{carb} > 0.8, yellow) and the meters, boreholes (bh), and clusters (cl) of each category. Unit names follow GSWA nomenclature (**Section S3**). "Other" combines the Capricorn, Pinjarra, and Paterson Orogens, the Madura Province, four boreholes in the Marymia Inlier of the Yilgarn Craton, which has no terrane assignment on the GSWA 1:10 M map, and basement beneath basin cover.

3.2 Downhole variation in mineral state

Weathering clays are confined to the top of the logs. The clay-rich share of all core falls from 0.63 in the uppermost 25 m to ≤ 0.02 below 150 m, and within ultramafic meters from 0.39 to 0.03 (**Figure 2a**). The surface clay zone has a median base of 42.5 m in the 95 boreholes whose logs include one (**Section S2.4**). Strong clay alteration can remove meters from the ultramafic set, but it does not raise X_{hyd}: only 108 of the 1,917 ultramafic meters above 100 m are clay-rich, and the clay-free ultramafic meters there have a mean X_{hyd} of 0.86. The mean X_{hyd} of ultramafic core declines through every successive interval, from 0.99 in the uppermost 25 m to below 0.3 deeper than 800 m, and the decline is shared by the two Yilgarn units with the most core (**Figure 2b**).

Because few boreholes reach the deepest intervals, we test the decline within boreholes. Below 100 m in 34 boreholes, the pooled slope of X_{hyd} is −0.038 per 100 m (95% interval −0.047 to −0.011), and −0.044 (−0.051 to −0.022) in the Eastern Goldfields Superterrane (**Figure 2c**). Individual slopes range from −0.18 to +0.18 per 100 m: 10 are negative with intervals excluding zero, 2 positive, and 22 indistinguishable from zero.

The pooled estimate is dominated by the longest-sampled boreholes: MTD026 holds 66% of its weight and, without it, the slope is −0.025 per 100 m, with an interval that still excludes zero (**Table S7b**). No clear pooled trend is detected in X_{carb} (+0.002 per 100 m; −0.025 to +0.014), although the difference between the two slopes is not resolved under borehole resampling (**Section S4.3**). On average within these boreholes, the serpentine share of the olivine–serpentine pair therefore decreases with depth below the weathering zone, whereas the talc–carbonate share shows no clear trend.

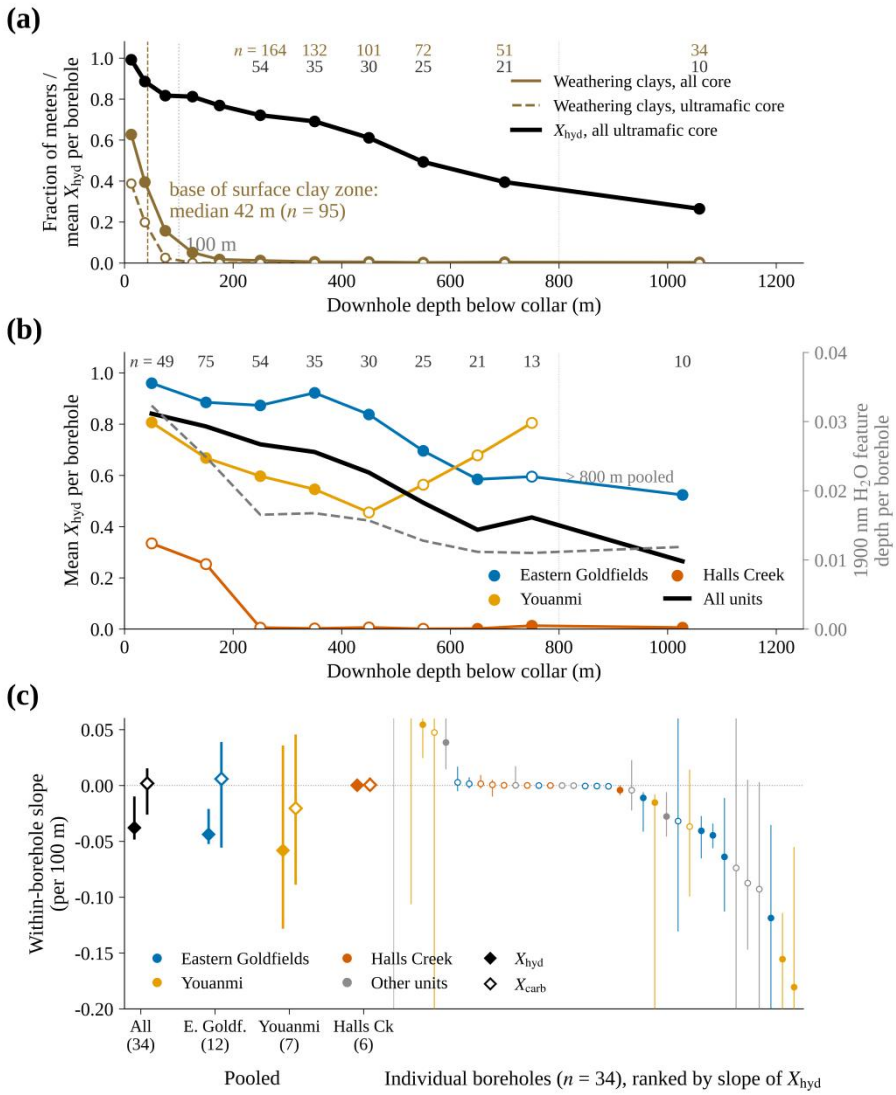


Figure 2. Weathering and mineral state of ultramafic core with downhole depth. Values are per-borehole means averaged over boreholes, and n is the number of boreholes per interval. (a) Fraction of clay-rich meters (SWIR smectite + kaolin > 0.2) in all core (solid brown) and in ultramafic meters (dashed brown), and mean X_{hyd} of ultramafic core (black). Above 200 m, n is 93–169 for all core and 8–59 for X_{hyd}. Vertical dashed line, median base of the surface clay zone (95 boreholes). (b) Mean X_{hyd} in 100 m intervals for the three tectonic units with the most boreholes and for all units (black). Intervals below 800 m are pooled at their median depth, and filled symbols have ≥ 5 boreholes. Dashed grey line (right axis), depth of the 1900 nm H_2O feature. (c) Within-borehole slopes below 100 m in 34 boreholes: pooled estimates (diamonds, 95% intervals) of X_{hyd} (filled) and X_{carb} (open) for all boreholes and for units with at least three. Right, individual boreholes ranked by X_{hyd} slope, filled where the 95% interval excludes zero.

3.3 Mineral state between clusters, host categories, and tectonic units

The 65 clusters with ≥ 50 m of ultramafic core plot along the edges of the olivine–serpentine–talc + carbonate ternary plot rather than in its interior (**Figure 3b**; **Table S5**): 28 have a talc + carbonate share above 0.8, 9 an olivine share above 0.5, and 7 a serpentine share above 0.8, and only one has both olivine and talc + carbonate above 0.3. Five of the six intrusion clusters have olivine shares of 0.64–0.99, among them the Sally Malay Suite, Panton Suite, and Giles Suite 1. The sixth, one of two Fraser Range Metamorphics clusters, has a serpentine share above 0.8, while the other is olivine-rich. Of the 37 greenstone-belt clusters, only 5 have an olivine share above 0.3, the largest being the Burtville Terrane (sub-division of the Eastern Goldfields Superterrane) greenstones cluster (2,050 m, 0.40). Of the 22 clusters in other mapped hosts, two have an olivine share above 0.3 (Windimurra Igneous Complex, 0.99; Euro Basalt, 0.44).

Per meter, the olivine-dominated fraction is 0.77 in the intrusions, 0.22 in the greenstone belts, and 0.09 in the other mapped hosts. Talc–carbonate-dominated meters are almost absent from the intrusions but form 0.56 of the greenstone-belt meters, and the other mapped hosts have a mean X_{carb} of 0.56 (**Table S6a**). Host category and tectonic unit covary: all greenstone-belt clusters lie in the Yilgarn Craton, and five of the six intrusion clusters lie in Proterozoic orogens or provinces.

Within tectonic units, boreholes of the same cluster are more alike than random groupings of the same boreholes: for X_{hyd}, the R^2 of borehole means is 0.89 about cluster means against 0.69 about unit means (47 boreholes in 15 multi-borehole clusters; permutation $p = 0.007$) and, for X_{carb}, 0.84 against 0.46 (130 boreholes, 37 clusters; $p = 0.0005$; **Table S7a**). The X_{hyd} test rests mainly on the Eastern Goldfields Superterrane and Youanmi Terrane, the only units with enough multi-borehole clusters to permute. Cluster means also explain more meter-level variance (0.63 for X_{hyd} and 0.71 for X_{carb}) than tectonic units (0.37, 0.22) or host categories (0.28, 0.17), but clusters are far more numerous, so these values do not compare the scales on equal terms (**Section S4.2**).

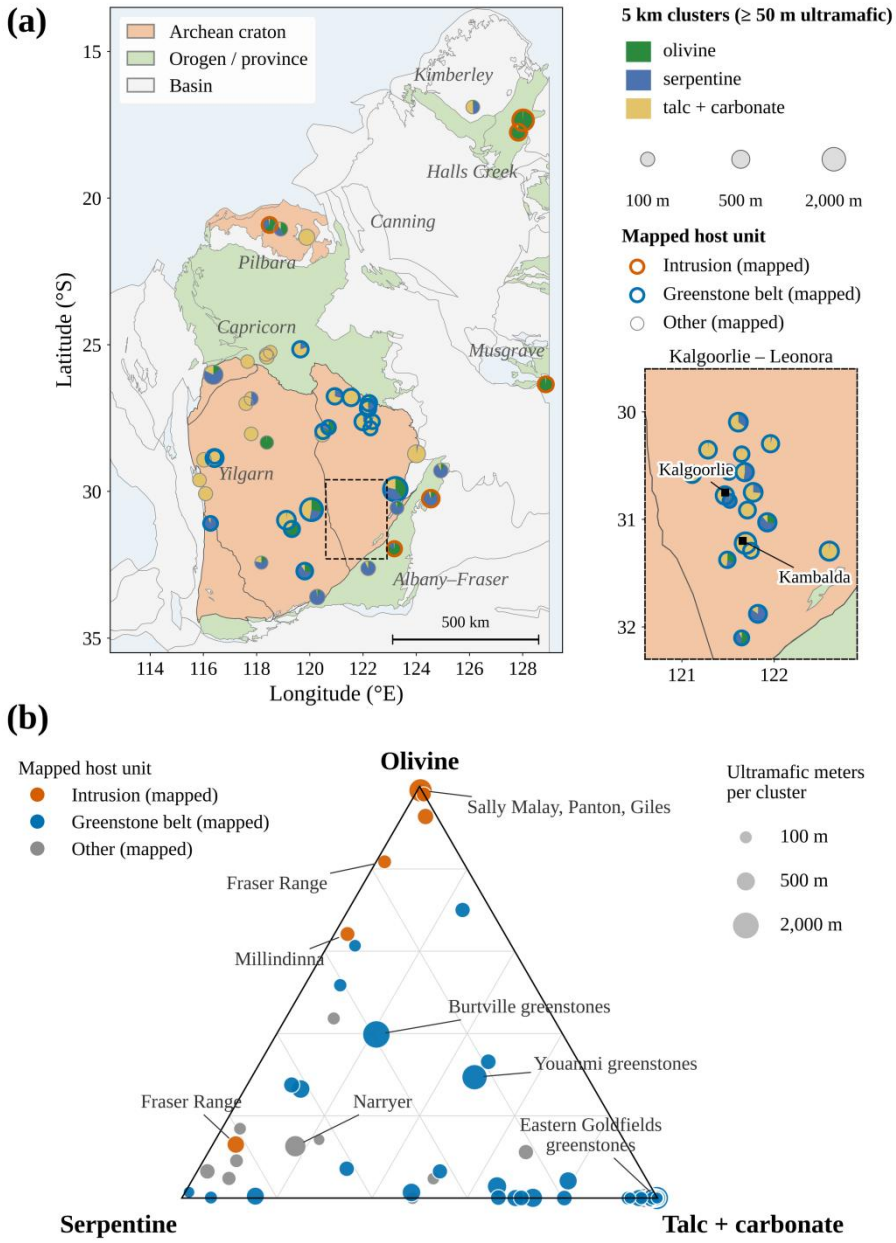


Figure 3. Mineral state of ultramafic core by borehole cluster and mapped host unit. (a) Each pie chart is a 5 km cluster with ≥ 50 m of ultramafic core (n = 65), showing the shares of olivine, serpentine, and talc + carbonate in its ultramafic meters. Pie area scales with ultramafic meters, and ring color gives the mapped host unit (**Table S5**). Inset, Kalgoorlie–Leonora region. (b) The same clusters in the olivine–serpentine–talc + carbonate ternary plot. Labels mark the largest cluster of each named host unit.

4. Discussion and Summary

4.1 Extensive talc–carbonate alteration in greenstone-hosted ultramafic rock

The intrusion clusters lie along the olivine–serpentine axis of the ternary plot (Figure 3b) with little talc or carbonate (mean X_{carb} 0.02), whereas greenstone-belt clusters spread across the field toward the talc–carbonate vertex (mean 0.62), so the two host categories differ in the type of alteration as well as its extent. The greenstone-belt pattern is consistent with the involvement of CO_2-bearing fluids: pre-metamorphic talc–carbonate rock is described at Agnew (Gole et al., 1987), and talc–carbonate margins surround serpentinite cores at Black Swan (Caruso et al., 2020; Hill et al., 2004). At Mulgarrie in the Eastern Goldfields Superterrane, komatiitic rocks were carbonated in two episodes of fluid flow along regional faults, both before peak metamorphism and gold mineralization (Davis et al., 2001), and carbonated ultramafic

rocks are preserved from the Archean to the present (Menzel et al., 2024). Part of the talc signal may be metamorphic, however, because carbonate forms only about a fifth of the talc + carbonate weight (median Cb/(Tlc + Cb) of 0.21; **Table S6a**) and the composition of the Other-MgOH group cannot be verified from the summary logs. Clusters in other mapped hosts are also rich in talc and carbonate, so this assemblage extends beyond areas mapped as greenstone. Because host category and tectonic unit covary, the data cannot distinguish whether the contrast reflects rock type (komatiite flows versus cumulate bodies) or tectonic setting, and exploration drilling in the two categories targeted different deposit types.

The coherence of clusters within tectonic units could reflect position in the same igneous body, a shared metamorphic grade, or shared fluid pathways, which our data cannot distinguish. Alteration can also vary strongly within one body, from 3% to 62% serpentinization in a Pyrenean lherzolite with a uniform temperature and burial history (Loiseau et al., 2024), and the two Fraser Range Metamorphics clusters differ similarly within one mapped host.

4.2 Less serpentine relative to olivine at depth

Reaction-induced cracking can, in some cases, sustain hydration but it is suppressed as effective pressure increases with depth (Malvoisin et al., 2017) and, in the Oman Drilling Project, alteration decreases downhole below a fully serpentinized upper 100–250 m (Kelemen et al., 2021; Templeton et al., 2024). The pooled decrease of X_{hyd} below 100 m is consistent with a similar pattern in Precambrian terranes, with olivine weights rising and serpentine weights falling downhole (**Table S7b**). The trend persists below the surface clay zones and when meters within 5 or 10 m of the spectral boundaries of ultramafic intervals are excluded, but it depends mainly on the longest-sampled boreholes. The depth of the 1900 nm H_2O feature also decreases downhole (from 0.032 at 0–100 m to 0.012 below 800 m; **Figure 2b**), consistent with, but not specific to, a lower serpentine content, because this feature records molecular water in several phases. Depths are along-hole, and the bodies have been buried, tilted, and exhumed since alteration, so the slope describes the present geometry of alteration within the drilled depths. Decreasing access of surface-derived fluids, cumulate zoning, and metamorphic olivine at depth could all contribute, and the result cannot be extrapolated to the 6–11 km generation window of Hutchinson et al. (2024), which may lie deeper still in cratons with low geothermal gradients (Etiope et al., 2026).

4.3 Implications for olivine-based source assessment

Within this archive and at drilled depths, olivine-bearing ultramafic core is unevenly distributed among greenstone-belt clusters. More than half of the greenstone-hosted core is talc–carbonate-dominated, and fewer than 1% of these intervals meet the olivine criterion. This low olivine share partly follows from the spectral definitions, but the important observations are the prevalence of these assemblages and their spatial distribution. Olivine-bearing core is concentrated in particular clusters (Table S5), where it may still represent a local hydrogen source. These findings challenge the premise of broadly retained olivine in greenstone-based hydrogen source models (Hutchinson et al., 2024).

The boreholes were drilled primarily for mineral exploration, which targets structurally complex and already altered ground. The archive is therefore likely biased toward altered rock, and the reported fractions describe sampled core rather than regional rock volumes. The results do not establish that most greenstone bodies lack olivine altogether, whether the remaining olivine is sufficient for hydrogen generation, or what lies below drilled depths. The spectral measurements also do not quantify olivine mass, Fe(II) content, or hydrogen yield, nor distinguish relict from metamorphic olivine. Non-detection of olivine today does not exclude past hydrogen generation. Other phases can also generate hydrogen, including ferroan brucite (Ellison et al., 2021) and pyroxene (Klein et al., 2013), and pyroxene may persist after olivine is altered. Olivine-depleted rock may thus keep a reduced generation potential that this study does not assess. These observations therefore constrain the spatial variability of remaining olivine, but local mineralogical characterization is still required to estimate reactive source rock, addressing a key uncertainty identified by Ballentine

et al. (2025).

4.4 Summary

In 18,692 m of ultramafic drill core from 218 Western Australian boreholes, olivine meets the spectral criterion in nearly all intrusion-hosted core but in only about a quarter of greenstone-hosted core, a contrast that holds per borehole, per cluster, and across olivine thresholds. More than half of the greenstone-hosted core is talc–carbonate-dominated and rarely olivine-bearing. Within tectonic units, neighboring boreholes share a similar mineral state beyond random grouping, and below 100 m the pooled serpentine share of the olivine–serpentine pair decreases with depth. This trend applies only to drilled depths, far shallower than the proposed 6–11 km generation window. Olivine preservation is therefore highly heterogeneous within mapped greenstone belts, with substantial differences in mineral state even between local borehole clusters. Together, these results show that remaining olivine in sampled greenstone-hosted ultramafic rocks is neither ubiquitous nor spatially uniform. Talc–carbonate-rich assemblages dominate much of the archive, while olivine-rich intervals are concentrated in particular borehole clusters. Greenstone-based hydrogen source models should therefore treat remaining olivine as a spatially variable, measurable component rather than assuming its widespread preservation.

Conflict of Interest

The authors declare no conflicts of interest relevant to this study.

Acknowledgement

Financial support and data provision through Australian Research Council Linkage project **LP220200912**. The hyperspectral logs analyzed here were acquired and released by the Geological Survey of Western Australia, a partner organization of the project. PWH publishes with the permission of the Executive Director of the Geological Survey of Western Australia. AF publishes with the permission of the CEO of Geoscience Australia.

Data Availability

All data are available in Zenodo (Li et al., 2026b) with DOI: https://doi.org/10.5281/zenodo.23629029

References

Andreani, M., Muñoz, M., Marcaillou, C., & Delacour, A. (2013). µXANES study of iron redox state in serpentine during oceanic serpentinization. *Lithos*, 178, 70–83. https://doi.org/10.1016/j.lithos.2013.04.008

Ballentine, C. J., Karolytė, R., Cheng, A., Sherwood Lollar, B., Gluyas, J. G., & Daly, M. C. (2025). Natural hydrogen resource accumulation in the continental crust. *Nature Reviews Earth & Environment*, 6(5), 342–356. https://doi.org/10.1038/s43017-025-00670-1

Barnes, S. J., & Fiorentini, M. L. (2012). Komatiite magmas and sulfide nickel deposits: A comparison of variably endowed Archean terranes. *Economic Geology*, 107(5), 755–780. https://doi.org/10.2113/econgeo.107.5.755

Beinlich, A., Plümper, O., Hövelmann, J., Austrheim, H., & Jamtveit, B. (2012). Massive serpentinite carbonation at Linnajavri, N-Norway. *Terra Nova*, 24(6), 446–455. https://doi.org/10.1111/j.1365-3121.2012.01083.x

Boreham, C. J., Sohn, J. H., Cox, N., Williams, J., Hong, Z., & Kendrick, M. A. (2021). Hydrogen and hydrocarbons associated with the Neoarchean Frog's Leg Gold Camp, Yilgarn Craton, Western Australia. *Chemical Geology*, 575, 120098. https://doi.org/10.1016/j.chemgeo.2021.120098

Caruso, S., Fiorentini, M. L., Barnes, S. J., LaFlamme, C. K., & Martin, L. A. J. (2020). Microchemical and sulfur isotope constraints on the magmatic and hydrothermal evolution of the Black Swan Succession, Western Australia. *Mineralium Deposita*, 55(3), 535–553.

https://doi.org/10.1007/s00126-019-00891-7

Christiansen, R., Sobh, M., Ostertag-Henning, C., Gianni, G., Saspiturry, N., Chevrot, S., Langenheim, V., García-Pintado, J., & Gabriel, G. (2026). Controls on natural hydrogen generation during serpentinization of mantle rocks. Nature Communications, 17, 5211. https://doi.org/10.1038/s41467-026-73920-5

Davies, K., Frery, E., Giwelli, A., Esteban, L., Keshavarz, A., & Iglauer, S. (2024). A natural hydrogen seep in Western Australia: Observed characteristics and controls. *Science and Technology for Energy Transition*, 79, 48. https://doi.org/10.2516/stet/2024043

Davis, B. K., Hickey, K. A., & Rose, S. (2001). Superposition of gold mineralisation on pre-existing carbonate alteration: Structural evidence from the Mulgarrie gold deposit, Yilgarn Craton. Australian Journal of Earth Sciences, 48(1), 131–149. https://doi.org/10.1046/j.1440-0952.2001.00846.x

Department of Energy, Mines, Industry Regulation and Safety. (2018). 1:500 000 State interpreted bedrock geology (DMIRS-016) [Dataset]. Government of Western Australia. https://catalogue.data.wa.gov.au/dataset/1-500-000-state-interpreted-bedrock-geology-dmirs-016

Department of Energy, Mines, Industry Regulation and Safety. (2023). Tectonic units 1:10 000 000 (DMIRS-084) [Dataset]. Government of Western Australia. https://catalogue.data.wa.gov.au/dataset/tectonic-units-1-10-000-000

Donzé, F.-V., Truche, L., Shekari Namin, P., Lefeuvre, N., & Bazarkina, E. F. (2020). Migration of natural hydrogen from deep-seated sources in the São Francisco Basin, Brazil. *Geosciences*, 10(9), 346. https://doi.org/10.3390/geosciences10090346

Ellis, G. S., & Gelman, S. E. (2024). Model predictions of global geologic hydrogen resources. *Science Advances*, 10(50), eado0955. https://doi.org/10.1126/sciadv.ado0955

Ellison, E. T., Templeton, A. S., Zeigler, S. D., Mayhew, L. E., Kelemen, P. B., Matter, J. M., & The Oman Drilling Project Science Party (2021). Low-temperature hydrogen formation during aqueous alteration of serpentinized peridotite in the Samail Ophiolite. *Journal of Geophysical Research: Solid Earth*, 126(6), e2021JB021981. https://doi.org/10.1029/2021JB021981

Etiope, G., Ellis, G. S., Ardakani, O. H., Boreham, C. J., Klitzke, P., Martín-Monge, A., Reis, H. L. S., Templeton, A. S., Kim, H. S., Gaucher, E., & Sissmann, O. (2026). Understanding the resource potential of natural hydrogen on Earth: Scientific gaps, uncertainties and recommendations. Earth-Science Reviews, 275, 105413. https://doi.org/10.1016/j.earscirev.2026.105413

Evans, B. W., Hattori, K., & Baronnet, A. (2013). Serpentinite: What, why, where? *Elements*, 9(2), 99–106. https://doi.org/10.2113/gselements.9.2.99

Falk, E. S., & Kelemen, P. B. (2015). Geochemistry and petrology of listvenite in the Samail ophiolite, Sultanate of Oman: Complete carbonation of peridotite during ophiolite emplacement. *Geochimica et Cosmochimica Acta*, 160, 70–90. https://doi.org/10.1016/j.gca.2015.03.014

Geymond, U., Loiseau, K., Roche, V., Pasquet, G., Revillon, S., Sougrati, M., & Moretti, I. (2025). Mössbauer spectroscopy: A key tool to quantify Fe-speciation and distribution in H_2-generating rocks. *Applied Geochemistry*, 187, 106399. https://doi.org/10.1016/j.apgeochem.2025.106399

Gole, M. J. (2014). Leaching of S, Cu, and Fe from disseminated Ni-(Fe)-(Cu) sulphide ore during serpentinization of dunite host rocks at Mount Keith, Agnew-Wiluna belt, Western Australia. Mineralium Deposita, 49(7), 821–842. https://doi.org/10.1007/s00126-014-0519-2

Gole, M. J., Barnes, S. J., & Hill, R. E. T. (1987). The role of fluids in the metamorphism of komatiites, Agnew nickel deposit, Western Australia. Contributions to Mineralogy and Petrology, 96(2), 151–162. https://doi.org/10.1007/BF00375229

Green, A. A., Green, D., Mason, P., & Berman, M. (2026). Joint unmixing of SWIR and TIR reflectance spectra for mineral composition. *Australian Journal of Earth Sciences*, 73(5), 720–729. https://doi.org/10.1080/08120099.2025.2464839

Grguric, B. A., Rosengren, N. M., Fletcher, C. M., & Hronsky, J. M. A. (2006). Type 2 deposits: Geology, mineralogy, and processing of the Mount Keith and Yakabindie orebodies, Western Australia. In S. J. Barnes (Ed.), *Nickel deposits of the Yilgarn Craton: Geology, geochemistry, and geophysics applied to exploration* (Society of Economic Geologists Special Publication 13, pp. 119–138). Society of Economic Geologists. https://doi.org/10.5382/SP.13.04

Haest, M., Cudahy, T., Laukamp, C., & Gregory, S. (2012). Quantitative mineralogy from infrared spectroscopic data. I. Validation of mineral abundance and composition scripts at the Rocklea channel iron deposit in Western Australia. *Economic Geology*, 107(2), 209–228. https://doi.org/10.2113/econgeo.107.2.209

Hill, R. E. T., Barnes, S. J., Dowling, S. E., & Thordarson, T. (2004). Komatiites and nickel sulphide orebodies of the Black Swan area, Yilgarn Craton, Western Australia. 1. Petrology and volcanology of host rocks. *Mineralium Deposita*, 39(7), 684–706.

https://doi.org/10.1007/s00126-004-0437-9

Hoatson, D. M., Jaireth, S., & Jaques, A. L. (2006). Nickel sulfide deposits in Australia: Characteristics, resources, and potential. *Ore Geology Reviews*, 29(3–4), 177–241. https://doi.org/10.1016/j.oregeorev.2006.05.002

Hughes, A., Britt, A., Pheeney, J., Morfiadakis, A., Kucka, C., Colclough, H., Munns, C., Senior, A., Cross, A., Hitchman, A., Cheng, Y., Walsh, J., & Jayasekara, A. (2025). *Australia's Identified Mineral Resources* 2024. Geoscience Australia. https://doi.org/10.26186/149861

Huntington, J., Quigley, M., Yang, K., Roache, T., Young, C., Roberts, I., Whitbourn, L., & Mason, P. (2006). A geological overview of HyLogging 18 000 m of core from the Eastern Goldfields of Western Australia. In *Sixth International Mining Geology Conference* (pp. 45–50). Australasian Institute of Mining and Metallurgy.

Hutchinson, I. P., Jackson, O., Stocks, A. E., Barnicoat, A. C., & Lawrence, S. R. (2024). Greenstones as a source of hydrogen in cratonic sedimentary basins. *Geological Society, London, Special Publications*, 547(1), 511–525. https://doi.org/10.1144/SP547-2023-39

Jackson, O., Lawrence, S. R., Hutchinson, I. P., Stocks, A. E., Barnicoat, A. C., & Powney, M. (2024). Natural hydrogen: Sources, systems and exploration plays. Geoenergy, 2(1), geoenergy2024-002. https://doi.org/10.1144/geoenergy2024-002

Kelemen, P. B., Leong, J. A., de Obeso, J. C., Matter, J. M., Ellison, E. T., Templeton, A., Nothaft, D. B., Eslami, A., Evans, K., Godard, M., Malvoisin, B., Coggon, J. A., Warsi, N. H., Pézard, P., Choe, S., Teagle, D. A. H., Michibayashi, K., Takazawa, E., Al Sulaimani, Z., & The Oman Drilling Project Science Team (2021). Initial results from the Oman Drilling Project Multi-Borehole Observatory: Petrogenesis and ongoing alteration of mantle peridotite in the weathering horizon. *Journal of Geophysical Research: Solid Earth*, 126(12), e2021JB022729. https://doi.org/10.1029/2021JB022729

Klein, F., Bach, W., Jöns, N., McCollom, T., Moskowitz, B., & Berquó, T. (2009). Iron partitioning and hydrogen generation during serpentinization of abyssal peridotites from 15°N on the Mid-Atlantic Ridge. *Geochimica et Cosmochimica Acta*, 73(22), 6868–6893. https://doi.org/10.1016/j.gca.2009.08.021

Klein, F., Bach, W., & McCollom, T. M. (2013). Compositional controls on hydrogen generation during serpentinization of ultramafic rocks. *Lithos*, 178, 55–69. https://doi.org/10.1016/j.lithos.2013.03.008

Kutzke, A., Eichstaedt, H., & Kahnt, R. (2022). Potential of hyperspectral-based geochemical predictions with neural networks for strategic and regional exploration improvement. *Australian Journal of Earth Sciences*, 69(8), 1197–1206. https://doi.org/10.1080/08120099.2022.2094465

Landgate. (2026). *Shared Location Information Platform* (SLIP) [Web service]. Government of Western Australia. https://www.data.wa.gov.au/

Laukamp, C., Rodger, A., LeGras, M., Lampinen, H., Lau, I. C., Pejcic, B., Stromberg, J., Francis, N., & Ramanaidou, E. (2021). Mineral physicochemistry underlying feature-based extraction of mineral abundance and composition from shortwave, mid and thermal infrared reflectance spectra. *Minerals*, 11(4), 347. https://doi.org/10.3390/min11040347

Laukamp, C., Mulè, S., Lau, I. C., Pejcic, B., Stromberg, J., Warren, P., Adams, C., Fazio, V., Francis, N., Hunt, A., Jiang, L., LeGras, M., Owen, N., Pinchand, T., Powell, H., & Shelton, T. (2026). The AuScope National Virtual Core Library infrastructure program—from vision to implementation. *Australian Journal of Earth Sciences*, 73(5), 630–641. https://doi.org/10.1080/08120099.2026.2693906

Lévy, D., Roche, V., Pasquet, G., Combaudon, V., Geymond, U., Loiseau, K., & Moretti, I. (2023). Natural H_2 exploration: Tools and workflows to characterize a play. Science and Technology for Energy Transition, 78, 27. https://doi.org/10.2516/stet/2023021

Li, J., Black, E., Miller, C. J., Tang, K., Mostaghimi, P., Feitz, A. J., Waite, T. D., & Armstrong, R. T. (2026a). Multi-modal characterization of ultramafic rock: Precursors relevant to serpentinization and hydrogen generation. Geoscience Frontiers, 17(2), 102220. https://doi.org/10.1016/j.gsf.2025.102220

Li, J., Haines, P., Feitz, A., Waite, T. D., & Armstrong, R. T. (2026b). *Data and code for "Do greenstone-belt ultramafic rocks retain olivine for hydrogen generation? Evidence from Western Australian drill core"* [Dataset]. Zenodo. https://doi.org/10.5281/zenodo.23629029

Loiseau, K., Aubourg, C., Petit, V., Bordes, S., Lefeuvre, N., Thomas, E., Hoareau, G., & Moretti, I. (2024). Hydrogen generation and heterogeneity of the serpentinization process at all scales: Turon de Técouère lherzolite case study, Pyrenees (France). *Geoenergy*, 2(1), geoenergy2023-024. https://doi.org/10.1144/geoenergy2023-024

Malvoisin, B., Brantut, N., & Kaczmarek, M.-A. (2017). Control of serpentinisation rate by reaction-induced cracking. *Earth and Planetary*

Science Letters, 476, 143–152. https://doi.org/10.1016/j.epsl.2017.07.042

McCollom, T. M., & Bach, W. (2009). Thermodynamic constraints on hydrogen generation during serpentinization of ultramafic rocks. *Geochimica et Cosmochimica Acta*, 73(3), 856–875. https://doi.org/10.1016/j.gca.2008.10.032

Menzel, M. D., Sieber, M. J., & Godard, M. (2024). From peridotite to listvenite – perspectives on the processes, mechanisms and settings of ultramafic mineral carbonation to quartz-magnesite rocks. Earth-Science Reviews, 255, 104828. https://doi.org/10.1016/j.earscirev.2024.104828

Menzel, M. D., Urai, J. L., Ukar, E., Hirth, G., Schwedt, A., Kovács, A., Kibkalo, L., & Kelemen, P. B. (2022). Ductile deformation during carbonation of serpentinized peridotite. *Nature Communications*, 13(1), 3478. https://doi.org/10.1038/s41467-022-31049-1

Mole, D. R., Fiorentini, M. L., Thébaud, N., Cassidy, K. F., McCuaig, T. C., Kirkland, C. L., Romano, S. S., Doublier, M. P., Belousova, E. A., Barnes, S. J., & Miller, J. (2014). Archean komatiite volcanism controlled by the evolution of early continents. *Proceedings of the National Academy of Sciences*, 111(28), 10083–10088. https://doi.org/10.1073/pnas.1400273111

Osselin, F., Soulaine, C., Fauguerolles, C., Gaucher, E. C., Scaillet, B., & Pichavant, M. (2022). Orange hydrogen is the new green. *Nature Geoscience*, 15(10), 765–769. https://doi.org/10.1038/s41561-022-01043-9

Rezaee, R. (2021). Assessment of natural hydrogen systems in Western Australia. *International Journal of Hydrogen Energy*, 46(66), 33068–33077. https://doi.org/10.1016/j.ijhydene.2021.07.149

Schodlok, M. C., Green, A., & Huntington, J. (2016). A reference library of thermal infrared mineral reflectance spectra for the HyLogger-3 drill core logging system. *Australian Journal of Earth Sciences*, 63(8), 941–949. https://doi.org/10.1080/08120099.2016.1234508

Schodlok, M. C., Whitbourn, L., Huntington, J., Mason, P., Green, A., Berman, M., Coward, D., Connor, P., Wright, W., Jolivet, M., & Martinez, R. (2016). HyLogger-3, a visible to shortwave and thermal infrared reflectance spectrometer system for drill core logging: Functional description. *Australian Journal of Earth Sciences*, 63(8), 929–940. https://doi.org/10.1080/08120099.2016.1231133

Schwarzenbach, E. M., Vogel, M., Früh-Green, G. L., & Boschi, C. (2021). Serpentinization, carbonation, and metasomatism of ultramafic sequences in the Northern Apennine Ophiolite (NW Italy). *Journal of Geophysical Research: Solid Earth*, 126(5), e2020JB020619. https://doi.org/10.1029/2020JB020619

Sherwood Lollar, B., Onstott, T. C., Lacrampe-Couloume, G., & Ballentine, C. J. (2014). The contribution of the Precambrian continental lithosphere to global H2 production. *Nature*, 516(7531), 379–382. https://doi.org/10.1038/nature14017

Sleep, N. H., Meibom, A., Fridriksson, Th., Coleman, R. G., & Bird, D. K. (2004). H2-rich fluids from serpentinization: Geochemical and biotic implications. *Proceedings of the National Academy of Sciences*, 101(35), 12818–12823. https://doi.org/10.1073/pnas.0405289101

Templeton, A. S., Ellison, E. T., Kelemen, P. B., Leong, J., Boyd, E. S., Colman, D. R., & Matter, J. M. (2024). Low-temperature hydrogen production and consumption in partially-hydrated peridotites in Oman: Implications for stimulated geological hydrogen production. *Frontiers in Geochemistry*, 2, 1366268. https://doi.org/10.3389/fgeoc.2024.1366268

Tutolo, B. M., & Tosca, N. J. (2023). Observational constraints on the process and products of Martian serpentinization. *Science Advances*, 9(5), eadd8472. https://doi.org/10.1126/sciadv.add8472

Ulrich, M., Rubatto, D., Hermann, J., Markmann, T. A., Bouvier, A.-S., & Deloule, E. (2024). Olivine formation processes and fluid pathways in subducted serpentinites revealed by in-situ oxygen isotope analysis (Zermatt-Saas, Switzerland). *Chemical Geology*, 649, 121978. https://doi.org/10.1016/j.chemgeo.2024.121978

Zeng, L., Sander, R., Salimzadeh, S., Lupton, N., & Camilleri, M. (2026). Orange hydrogen in Yilgarn Craton, Western Australia: Geochemical modeling on stimulated hydrogen production integrated with carbon dioxide mineralization. *International Journal of Hydrogen Energy*, 245, 155631. https://doi.org/10.1016/j.ijhydene.2026.155631

Zgonnik, V. (2020). The occurrence and geoscience of natural hydrogen: A comprehensive review. *Earth-Science Reviews*, 203, 103140. https://doi.org/10.1016/j.earscirev.2020.103140

Supplementary Information for

Extensive Olivine Depletion in Archean Greenstone Belts: Evidence from Drill Core and Implications for Natural Hydrogen Generation

Jiejie Li[1], Peter W Haines[2], Andrew Feitz[3], T. David Waite[1], and Ryan T. Armstrong[1]

[1]School of Civil and Environmental Engineering, UNSW Sydney, Sydney, Australia, [2]Geological Survey of Western Australia, Perth, Australia, [3]Geoscience Australia, Canberra, Australia.

Contents

Sections S1 to S5
Tables S1 to S8

Introduction

This supplementary information documents the data and methods behind the main article. Section S1 describes the screening of the National Virtual Core Library for ultramafic drill core. Section S2 gives the per-meter mineralogy, the definitions of the two assemblage indices, and their sensitivity to the thresholds used. Section S3 describes how boreholes were assigned to tectonic units, mapped host units, and clusters. Section S4 gives the statistical analysis of the within-borehole trends and of the variance explained by tectonic unit, host category, and cluster. Section S5 reports the robustness of the olivine criterion and of the contrast between host categories. Tables S1 to S8 give the screening results, the sensitivity tests, the cluster inventory, the group statistics, and the robustness results.

Section S1. Screening of the National Virtual Core Library for ultramafic drill core

The National Virtual Core Library (NVCL) hosts continuous hyperspectral scans of drill core acquired with the HyLogger instrument suite by the state and territory geological surveys and CSIRO (Schodlok, Whitbourn, et al., 2016; Laukamp et al., 2026). We queried every NVCL borehole published through the state and territory data services and retained, for each borehole, all datasets carrying a thermal-infrared (TIR) mineral log. Neither olivine nor pyroxene is classified by the short-wave infrared (SWIR) mineral system, so both are recorded only in the TIR logs; datasets without a TIR log therefore cannot be screened for ultramafic mineralogy and were excluded at the first step. Of 6,705 dataset records returned, 1,605 had no usable TIR result: 1,597 listed no TIR log (1,596 with a SWIR log, one with neither) and a further 8 listed a TIR log that returned no valid spectra. This left 5,100 datasets with a usable TIR log. For each retained dataset we downloaded the "system-joined" TIR class log (Grp1 sjCLST; Grp1 ujCLST where the joined product was unavailable) binned at 1 m downhole spacing. For each 1 m bin the service returns the number of individual spectra assigned to each dominant mineral-group class. We summed these counts over the whole dataset, discarding spectra flagged INVALID (Schodlok, Green, & Huntington, 2016), and expressed each class as a fraction of all valid spectra. Class frequencies are therefore proportions of valid spectra, not mass fractions or lengths of core. Four classes define the ultramafic mineral system:

OLIVINE, SERPENTINE, PYROXENE and OTHER-MGOH (talc and other Mg-OH phases; chlorite and amphibole are separate classes). Their sum is the ultramafic index (UM).

Datasets were assigned to one of six mutually exclusive categories, tested in the order listed:

- A (partially serpentinized): olivine ≥ 0.05 and serpentine ≥ 0.05
- B (olivine-bearing, weakly altered): olivine ≥ 0.05
- C (serpentinized): serpentine ≥ 0.15
- D (talc–MgOH dominated): OTHER-MGOH ≥ 0.15
- E (pyroxene dominated): pyroxene ≥ 0.20
- F (minor ultramafic component): UM ≥ 0.05

Thresholds are deliberately permissive at the lower bound (0.05, i.e. 5% of valid spectra) so that thin or sparsely intersected ultramafic units are not lost, and are raised for the single-mineral categories (0.15–0.20), where a low frequency is less diagnostic. A dataset failing all six tests is not a candidate. The screen returned 603 candidate datasets: 13 in A, 21 in B, 48 in C, 81 in D, 70 in E and 370 in F, from 1,376,319 logged meters in total.

The 34 datasets in categories A and B, those recording primary olivine, are almost entirely confined to Western Australia (33 of 34); the single exception is a 61 m Queensland intersection with UM = 0.082. This concentration reflects both the Archean ultramafic endowment of the Yilgarn and Pilbara cratons and the exploration history that generated the cores (Hoatson et al., 2006; Barnes & Fiorentini, 2012; Geoscience Australia, 2025), and it is the basis for restricting the analysis in the main text to Western Australia.

Table S1. Screening of the National Virtual Core Library for ultramafic drill core.

Custodian	Holes	Datasets	TIR logs	Logged meters	A	B	C	D	E	F	Candidates
Geological Survey of Western Australia	1,897	2,008	1,962	608,038	13	20	34	74	28	190	359
Geological Survey of South Australia	2,058	1,831	1,414	333,025	0	0	9	4	27	102	142
Geological Survey of New South Wales	1,250	1,256	919	205,898	0	0	1	2	4	24	31
Northern Territory Geological Survey	565	578	270	72,030	0	0	0	1	2	9	12
Geological Survey of Queensland	586	537	231	67,521	0	1	0	0	5	13	19
Mineral Resources Tasmania	485	490	304	89,807	0	0	4	0	4	32	40
CSIRO	5	5	0	0	0	0	0	0	0	0	0
Total	**6,846**	**6,705**	**5,100**	**1,376,319**	**13**	**21**	**48**	**81**	**70**	**370**	**603**

Note. "Holes" is the number of boreholes returned by each service, with or without a dataset; "TIR logs" counts datasets whose TIR class log returned at least one valid spectrum; "Logged meters" is the number of 1 m bins containing at least one valid TIR spectrum, summed over those datasets. Categories A–F are defined in **Section S1; they are mutually exclusive, were tested in the order shown, and count each dataset under its own category. Nine of the 359 Western Australian candidate records are scans of drill chips or cuttings. Victoria returned no data during screening (NVCL data service unavailable).*

Section S2. Per-meter mineralogy and assemblage indices

S2.1 Data product

For each of the 359 Western Australian candidate records identified in **Section S1** we used the corresponding GSWA HyLogger Summary Mineral Log (one file per scan). Each log reports, at 1 m downhole intervals, the abundance of 23

thermal-infrared (TIR) mineral groups and an invalid class from jCLST spectral unmixing against the HyLogger-3 TIR reference library (Schodlok, Green, & Huntington, 2016), of 13 shortwave-infrared (SWIR) mineral groups and an invalid class from TSA+ unmixing, and a set of spectral-feature scalars. Each file records a minimum bin weight of 0.05 for the unmixing (*Bin_min_threshold*); interval values below this level are nevertheless common (71% of non-zero serpentine values), so interval abundances are not themselves thresholded at 0.05. In 355 files the unmixing is the automated "System" result and in four the geologist-refined "User" result; both were read. These logs are a different product from the whole-hole class frequencies of individual spectra used for screening in **Section S1**, and the two are not compared.

S2.2 Definitions

The ultramafic-interval criterion and the indices X_{hyd} and X_{carb} are defined in **Section 2.1** of the main text.. Tlc denotes the Other-MgOH group of the log, which comprises talc and other Mg-OH phases (brucite is recorded in the SWIR only). The first condition of the criterion alone admits 21,641 m in 250 records, including 2,751 m of carbonate-dominated intervals (Cb ≥ 0.5), mostly in sedimentary units such as the Edmund Group and Coomberdale Subgroup and in carbonate-altered mafic rocks such as the Carrington Suite and Kulkatharra Dolerite. The second condition removes 2,949 m in which carbonate dominates over the Mg-silicate assemblage and leaves 18,692 m in 219 records from 218 boreholes (**Table S2**). The criterion targets olivine–serpentine–talc assemblages: by design it also excludes ultramafic rock carbonated to a quartz–carbonate assemblage in which no Mg-silicate remains, and pyroxenite lies outside it. The lithology of individual intervals has not been verified against core descriptions. The denominator threshold of 0.1 for X_{hyd} is twice the minimum bin weight recorded in the logs, so that no ratio is formed from trace abundances; X_{hyd} is defined in 9,762 m. X_{carb} is defined in every ultramafic meter and is divided into Mg-silicate-dominated (< 0.2), mixed (0.2–0.8) and talc–carbonate-dominated (> 0.8) classes with the same cut-offs as X_{hyd} (**Table S4**). Ninety of the 3,072 olivine-dominated meters have Tlc + Cb ≥ 0.5; a low X_{hyd} therefore indicates that olivine dominates over serpentine, not that the interval is free of other alteration.

Table S2. Effect of the ultramafic-interval criterion on the per-meter data set. Srp, Ol, Tlc and Cb are the jCLST weights of the serpentine, olivine, Other-MgOH and carbonate groups. Olivine-dominated fraction is the share of meters with X_{hyd} defined that have $X_{hyd} < 0.2$. R^2 is the fraction of the variance of X_{carb} = (Tlc + Cb)/(Srp + Ol + Tlc + Cb) explained by the group means of tectonic unit or of 5 km cluster (a connected group of boreholes in which each lies within 5 km of another); the number of clusters is far larger than the number of units, which favors the cluster R^2.

Ultramafic-interval criterion	Ultramafic meters	Records	Boreholes	5 km clusters	Meters with Cb ≥ 0.5	Olivine-dominated fraction (X_{hyd} < 0.2)	R^2 of X_{carb}, tectonic unit	R^2 of X_{carb}, 5 km cluster
Single condition: Srp + Ol + Tlc + Cb ≥ 0.5	21,641	250	249	126	2,751	0.31	0.27	0.72
Two conditions, first threshold 0.4: Srp + Ol + Tlc + Cb ≥ 0.4 and Srp + Ol + Tlc ≥ 0.3	21,448	231	230	117	69	0.36	0.23	0.72
Two conditions, first threshold 0.5 (adopted): Srp + Ol + Tlc + Cb ≥ 0.5 and Srp + Ol + Tlc ≥ 0.3	18,692	219	218	110	69	0.31	0.22	0.71
Two conditions, first threshold 0.6: Srp + Ol + Tlc + Cb ≥ 0.6 and Srp + Ol + Tlc ≥ 0.3	16,040	210	209	106	69	0.29	0.20	0.70

**Note: The second condition removes 2,949 m, of which 2,682 m have Cb ≥ 0.5; these meters are carbonate-dominated rock that is not ultramafic (sedimentary carbonate and carbonate-altered mafic rock).*

S2.3 Sensitivity

Table S2 varies the ultramafic criterion (with and without its second condition, and with the first threshold at 0.4, 0.5 and 0.6), **Table S3** varies the denominator threshold of X_{hyd} from 0.02 to 0.30, and **Table S4** varies the class cut-offs. The olivine-dominated fraction is 0.30–0.32 across the denominator thresholds, 0.29–0.36 across the first threshold of the criterion and 0.28–0.35 across the cut-offs; the number of boreholes with ≥ 30 m of ultramafic core and ≥ 10 m of olivine-dominated meters is 27–33, and the pattern of the olivine-dominated fraction by depth interval is the same in every row. The intermediate fractions (0.13–0.31 for X_{hyd}, 0.06–0.18 for X_{carb}) change with the width of the intermediate class by construction and are reported for the adopted cut-offs only. The second condition of the criterion changes the size of the data set (2,949 m, 31 records, 16 clusters) but not the olivine-dominated fraction; without it, the variance of X_{carb} explained by tectonic unit rises from 0.22 to 0.27, because the removed carbonate-dominated intervals are concentrated in particular units, while the variance explained by 5 km cluster is unchanged (0.71–0.72).

Table S3. Sensitivity of the X_{hyd} statistics to the denominator threshold below which X_{hyd} = Srp/(Srp + Ol) is left undefined. All rows use the adopted ultramafic criterion (18,692 m) and the 0.2/0.8 cut-offs. Depth intervals refer to the midpoint depth of each 1 m interval below the collar.

Denominator threshold (Srp + Ol ≥)	Meters with X_{hyd} defined	Olivine-dominated fraction (< 0.2)	Intermediate fraction (0.2–0.8)	Boreholes with ≥ 30 m ultramafic core and ≥ 10 m olivine-dominated	Olivine-dominated fraction by midpoint depth interval (m)					
					0–50	50–100	100–200	200–400	400–800	> 800
0.02	10,386	0.30	0.19	29	0.04	0.05	0.17	0.18	0.37	0.81
0.05	10,022	0.31	0.19	29	0.05	0.05	0.18	0.18	0.38	0.82
0.10 (adopted)	9,762	0.31	0.20	29	0.05	0.05	0.19	0.19	0.38	0.83
0.15	9,595	0.32	0.20	29	0.06	0.05	0.19	0.19	0.38	0.84
0.20	9,432	0.32	0.20	29	0.06	0.05	0.19	0.19	0.38	0.85
0.30	9,162	0.32	0.20	28	0.06	0.05	0.19	0.19	0.38	0.85

**Note: The adopted value (0.10) is a rule against forming ratios from small denominators. It is twice the Bin_min_threshold recorded in the log headers (0.05), a parameter of the unmixing that is not a detection limit for interval abundances.*

Table S4. Sensitivity of the reaction-state fractions to the cut-offs that separate the lower class (index below the first value), the intermediate class and the upper class (index above the second value). For X_{hyd} the classes are olivine-dominated, intermediate and serpentine-dominated; for X_{carb} = (Tlc + Cb)/(Srp + Ol + Tlc + Cb) they are Mg-silicate-dominated, mixed and talc–carbonate-dominated. All rows use the adopted ultramafic criterion and the 0.10 denominator threshold (X_{hyd} defined on 9,762 m; X_{carb} on all 18,692 m).

Cut-offs (lower / upper)	Olivine-dominated fraction	Serpentine-dominated fraction	Intermediate fraction, X_{hyd}	Mixed fraction, X_{carb}	Talc–carbonate-dominated fraction, X_{carb}	Boreholes with ≥ 30 m ultramafic core and ≥ 10 m olivine-dominated	Olivine-dominated fraction by midpoint depth interval (m)					
							0–50	50–100	100–200	200–400	400–800	> 800
0.1 / 0.9	0.28	0.41	0.31	0.18	0.47	27	0.05	0.05	0.15	0.14	0.35	0.78

Cut-offs (lower / upper)	Olivine-dominated fraction	Serpentine-dominated fraction	Intermediate fraction, X_{hyd}	Mixed fraction, X_{carb}	Talc–carbonate-dominated fraction, X_{carb}	Boreholes with ≥ 30 m ultramafic core and ≥ 10 m olivine-dominated	Olivine-dominated fraction by midpoint depth interval (m)					
							0–50	50–100	100–200	200–400	400–800	> 800
0.2 / 0.8 (adopted)	0.31	0.49	0.20	0.10	0.49	29	0.05	0.05	0.19	0.19	0.38	0.83
0.3 / 0.7	0.35	0.52	0.13	0.06	0.50	33	0.05	0.06	0.21	0.23	0.42	0.86

S2.4 Surface weathering

A meter is clay-rich where the SWIR (TSA+) weights of smectite + kaolin exceed 0.2; the indicator is evaluated on all 83,488 logged meters of the 218 boreholes, not only on ultramafic meters, and does not enter the TIR-based ultramafic criterion or X_{hyd}. The surface clay zone of a borehole is the uppermost contiguous run of 10 m windows with ≥ 50% clay-rich meters that begins within 20 m of the first logged meter; its base is the deepest meter of the run. Ninety-five boreholes have such a zone, with the base at a median depth of 42.5 m (interquartile range 25.5–69.0 m, maximum 154.5 m). Of the 123 boreholes without one, 117 have no clay-rich run anywhere in the log: in 96 of them the log begins more than 30 m below collar (median 119.5 m), so that the weathered interval was not scanned, and the remaining 21 begin shallower and contain no clay-rich run; the other 6 have a clay-rich run deeper than 20 m below the top of the log that is treated as alteration. Varying the threshold (0.1–0.3), window (5–20 m), window fraction (0.3–0.7) or tolerance (10–40 m) gives 87–104 boreholes with a zone and a median base of 37.5–48.5 m.

Weathering removes meters from the ultramafic inventory rather than raising X_{hyd}: only 108 of the 1,917 ultramafic meters in the uppermost 100 m, and 5 of the 16,775 below, are clay-rich, and the clay-free ultramafic meters in the uppermost 100 m have a mean X_{hyd} of 0.86 (677 m with X_{hyd} defined, 36 m olivine-dominated). In the 40 boreholes with olivine-dominated meters the shallowest olivine-dominated meter lies at a median depth of 232 m, and in all 24 that also have a surface clay zone it lies below the base of the zone (median 280 m deeper). The 100 m cut used for the within-borehole slopes (**Figure 2c**) lies below the clay zone in each of the 34 boreholes analyzed; 7 of the 95 zones extend below 100 m.

Section S3. Borehole attributes: tectonic units, clusters and host units

S3.1 Tectonic units and host units of boreholes

Each borehole was located by its NVCL collar coordinates and assigned by point-in-polygon query, to two Geological Survey of Western Australia map layers served through the Shared Location Information Platform (Landgate, 2026): the Tectonic units 1:10 000 000 layer (DMIRS-084; Department of Energy, Mines, Industry Regulation and Safety, DEMIRS, 2023), which gives the tectonic unit used in **Figures 1**–**3** and named as in the **Figure 1** caption, and the 1:500 000 State interpreted bedrock geology layer (DMIRS-016; DEMIRS, 2018), which gives the mapped bedrock unit at the collar, here called the host unit. The query results and the script that derives the borehole attribute table from them are part of the data package. All 218 boreholes with ultramafic core received both attributes; their host units comprise 52 named bedrock units. The host unit describes the map polygon at the collar, not the rock logged at depth: ultramafic bodies too small to be shown at 1:500 000 are absorbed into the surrounding unit, so 15 boreholes with ultramafic core are mapped as Yilgarn Craton granites, and an inclined borehole may leave its collar unit at depth. Depths are downhole depths below the collar as recorded in the Summary Mineral Logs; dip and azimuth are not part of the products used, so no conversion to vertical depth was made.

S3.2 Borehole clusters and their host-unit classes

Boreholes in a mineral prospect are typically a few hundred meters apart and intersect the same body. To compare bodies rather than boreholes, the 218 boreholes were grouped into clusters, defined as connected components of the graph that links any two collars separated by a great-circle distance of 5 km or less. This gives 110 clusters: 65 single boreholes and 45 groups of 2–12 boreholes, the largest near Kambalda; the largest separation between two boreholes of one cluster is 7.04 km. Linking radii of 1, 2 and 10 km give 135, 127 and 101 clusters. Clusters, not boreholes, are the sampling units of the between-body comparisons in this Section.

The host unit of a cluster is the bedrock unit that hosts the largest number of its ultramafic meters; 9 of the 110 clusters contain more than one bedrock unit. Host units were classed by name alone. Four units described in the bedrock geology layer as layered mafic–ultramafic intrusions (Sally Malay Suite, Panton Suite, Giles Suite 1, Millindinna Intrusion) and two units described as high-grade mafic meta-igneous rocks (Tickalara Metamorphics, Fraser Range Metamorphics) (DEMIRS, 2018) form the class "intrusion"; units whose name contains "greenstone" (the Eastern Goldfields Superterrane, Youanmi Terrane, Burtville Terrane and South West Terrane greenstones) form the class "greenstone belt", all other units form the class "other". The three classes hold 9, 49 and 52 clusters with 2,094, 12,886 and 3,712 ultramafic meters. The rule was not adjusted for lithology; units whose descriptions in the bedrock geology layer would place them differently are identified in the note to **Table S5b**. **Figure 3** shows the 65 clusters with at least 50 ultramafic metres (17,862 m); the remaining 45 clusters hold 830 m. **Table S5** lists all 110 clusters with their attributes (**Table S5a**) and all 48 cluster-level host units with their class (**Table S5b**).

Section S4. Statistical analysis

S4.1 Within-borehole trends

The slopes of **Figure 2c** use the meters below 100 m, which lie beneath the surface clay zone in every borehole considered (**Section S2.4**). A borehole is included when it has at least 30 such meters with X_{hyd} defined spanning at least 200 m of depth; 34 boreholes qualify. The slope of a borehole is the least-squares slope of X_{hyd} on depth per 100 m. Because neighbouring meters are not independent, its 95% interval comes from a moving-block bootstrap, the sequence of defined meters is reassembled from randomly placed blocks of 10 successive meters, the slope is recomputed, and the 2.5th and 97.5th percentiles of 1,000 such recomputations are taken. A slope is called negative or positive only when this interval excludes 0 (10 and 2 of the 34 boreholes; 22 are indistinguishable from zero). The pooled slope of a group is the common slope after subtracting the borehole means of X_{hyd} and depth, which removes the between-borehole differences of **Section 3.3**. Its 95% interval is obtained by drawing boreholes with replacement from the group, recomputing the pooled slope on each such set, and taking the 2.5th and 97.5th percentiles over 2,000 sets. Pooled slopes are given for all 34 boreholes and for the three units with at least three of them, and the same estimator is applied to X_{carb} over every ultramafic meter below 100 m of the same boreholes.

S4.2 Variance explained by tectonic unit, host-unit class and cluster

R^2 in **Table S6b** is one minus the ratio of the within-group to the total sum of squares over the meters in which the index is defined: X_{hyd} in 9,762 m from 126 boreholes and 75 clusters, X_{carb} in all 18,692 m from 218 boreholes and 110 clusters. Host-unit class is the class of the cluster's host unit (**Section S3.2**), so the classes are unions of clusters and their R^2 cannot exceed the cluster R^2. A larger number of groups favors a higher R^2, so the comparison in **Section 3.3** is between the two coarse groupings (9 tectonic units, 3 classes), and the cluster R^2 is the value reached when every body is its own group. For X_{carb} and the adopted criterion it is the quantity given in **Table S2**. **Table S6a** lists the group inventories and index

means used in **Sections 3.1** and **3**.

S4.3 Robustness of the between-cluster and within-borehole results

Table S7a tests at the borehole level whether boreholes of the same cluster resemble each other more than their tectonic unit implies. Boreholes with at least 10 m of the index defined enter with their mean, clusters with fewer than two such boreholes are dropped. The R^2 of the borehole means about cluster means is compared with the R^2 about tectonic-unit means and with a null distribution obtained by permuting cluster labels among the boreholes of each unit ($N = 2{,}000$; $p = (k + 1)/(N + 1)$, k being the permutations that reach the observed R^2). For X_{hyd} (47 boreholes, 15 clusters) the cluster R^2 is 0.89, the unit R^2 0.69 and the 95th percentile of the null 0.85, $p = 0.0070$; the standard deviation among boreholes is 0.12 within clusters and 0.21 within units. Only the Eastern Goldfields Superterrane (22 boreholes, 8 clusters) and the Youanmi Terrane (9 boreholes, 3 clusters) contain more than one multi-borehole cluster, so the permutation is informative only there. The result holds for means restricted to meters below 100 m ($p = 0.0085$) and for X_{carb} (130 boreholes, 37 clusters, $p = 0.0005$).

Table S7b recomputes the pooled slopes of **Section 2.3** on the common meters of the 34 boreholes (6,637 m below 100 m with X_{hyd} defined) for both indices and the four mineral weights, with intervals from resampling boreholes and from resampling the 23 clusters. Olivine rises by 0.036 and serpentine falls by 0.027 per 100 m; talc, carbonate and X_{carb} have no slope distinguishable from 0. The paired difference between the X_{hyd} and X_{carb} slopes is −0.034 per 100 m; its interval includes zero under borehole resampling (−0.044 to +0.001) and excludes it under cluster resampling (−0.047 to −0.004). Since 56% of the common meters lie within 10 m of a meter that fails the ultramafic criterion, the X_{hyd} slope was recomputed without meters within 5 m and within 10 m of such a meter, in the boreholes that still meet the selection of **Section 2.3**. For these boreholes the slope moves from −0.040 to −0.044 and from −0.040 to −0.042 per 100 m, with intervals that exclude zero under both resamplings. The boundary is spectral, not a logged contact. Because each borehole is weighted by the number and the spread of its sampled depths, leverage is concentrated: MTD026, with 1,197 meters between 100 and 1,468 m, holds 65.9% of the weight of the X_{hyd} slope and the five highest-weighted boreholes 84.0%. Its own slope is −0.045. Excluding it the pooled slope is −0.025 per 100 m in 33 boreholes, its interval excluding zero under both resamplings.

Section S5. Robustness of the olivine criterion and of the host-category contrast

S5.1 Spectral background of the olivine weight

To describe the olivine weight in rock that should not contain olivine, we read the TIR weights of all 23 mineral groups for every logged meter of the 359 candidate records and selected meters without any condition on the olivine weight: quartz-rich meters (silica ≥ 0.7) and quartz-bearing felsic meters (silica ≥ 0.3 and silica + plagioclase + K-feldspar + white mica ≥ 0.7), each with serpentine + Other-MgOH + carbonate < 0.1. Forsterite and quartz do not coexist at equilibrium, so these meters are taken as olivine-free on petrological grounds; the selection leaves room for olivine weights of up to 0.3. Ol never exceeds 0.05 in the 4,856 quartz-rich meters (209 boreholes; maximum 0.004) or in the 30,139 quartz-bearing felsic meters (304 boreholes; maximum 0.047), and exceeds 0.02 in 0.05% of the latter (Table S8d). This describes the spectral background of the olivine weight in quartz-bearing rock; it is not an independent validation of the olivine criterion, because no meter was checked mineralogically, and it says nothing about whether olivine is missed where it is mixed with serpentine, talc, or carbonate. Confirming the criterion requires quantitative mineralogy of representative core, such as XRD with Rietveld refinement or thin-section point counts, which is beyond the scope of this archive-based study.

S5.2 Olivine threshold

Table S8a repeats the host-category comparison of Section 3.1 with Ol > 0.02, 0.05, 0.10, and 0.15. The olivine-bearing share of ultramafic meters falls from 98.9% to 88.0% in intrusion-hosted core and from 25.8% to 19.9% in greenstone-hosted core, so the ratio between the two categories stays between 3.8 and 4.4. Of the talc–carbonate-dominated meters (X_{carb} > 0.8), 1.6% meet the lowest threshold and 0.02% the highest.

S5.3 Weighting per meter, per borehole, and per cluster

The per-meter shares of Section 3.1 weight each borehole by its logged ultramafic length. Table S8b also weights each borehole and each 5 km cluster equally, with 95% intervals from 2,000 resamples of whole clusters within each category; a cluster drawn more than once enters each resample as separate copies. The intrusion category is 96.7% (87.5–100%) olivine-bearing per meter, 98.5% (92.7–100%) per borehole, and 97.5% (92.6–100%) per cluster; the greenstone-belt category 23.9% (10.0–35.1%), 11.9% (5.5–20.1%), and 17.8% (9.6–26.5%). Of the intrusion-hosted boreholes 93% hold ≥ 10 m of olivine-bearing core, against 16.8% of the greenstone-hosted boreholes, and all 9 intrusion clusters but 18.4% of the 49 greenstone-belt clusters have an olivine-bearing share of at least 0.5. The per-borehole share is the mean, over boreholes, of the olivine-bearing fraction of each borehole's ultramafic meters, not the fraction of boreholes containing olivine; for the greenstone-belt category it is lower than the per-meter share because the longest-logged greenstone-hosted boreholes are among the more olivine-rich.

S5.4 Leave-out tests

Table S8c removes the largest cluster, the longest borehole, or each cluster in turn. For the greenstone-belt category, removing the largest cluster (Burtville Terrane greenstones, 2,050 m) gives 18.5%, removing borehole MTD026 (1,301 m) 17.3%, and removing any single cluster 18.5–25.9%. Excluding the Eastern Goldfields Superterrane raises the greenstone-belt share to 38.3% and excluding the Youanmi Terrane lowers it to 18.7%, so the share varies between tectonic units but remains far below that of the intrusion category, which stays between 93.4% and 99.9% when any single intrusion cluster is removed (95.9% without its longest borehole, SMD157-A, 426 m).

Table S5. Inventory of the 1105 km borehole clusters with ultramafic core (18,692 m, 218 boreholes), numbered from north to south. (a) Clusters. (b) Mapped host units and their classification.

(a) Clusters.

No.	Tectonic unit	Mapped host unit (1:500 000)	Class	Bore-holes	Ultramafic m	m with X_{hyd}	Olivine-dominated m (X_{hyd} < 0.2)	Olivine	Serpentine	Talc + carb.	Max. depth	Lat. (°S)	Lon. (°E)	Fig. 3
1	Other	King Leopold Sandstone	Other	2	73	46	0	0.05	0.45	0.51	276	16.90	126.13	●
2	Halls Creek	Sally Malay Suite	Intrusion	7	1,045	1,045	1,042	0.99	0.00	0.01	1,340	17.35	128.02	●
3	Other	Fitzroy Volcanics	Other	3	31	31	0	0.05	0.76	0.19	79	17.56	124.86	–
4	Other	Fairfield Group	Other	1	44	44	0	0.04	0.83	0.13	142	17.67	124.93	–
5	Halls Creek	Panton Suite	Intrusion	1	235	234	234	0.93	0.02	0.05	1,062	17.76	127.84	●
6	Halls Creek	Marboo Formation	Other	2	2	2	0	0.01	0.89	0.09	151	18.32	126.10	–
7	Pilbara	Millindinna Intrusion	Intrusion	1	157	157	31	0.64	0.33	0.03	380	20.92	118.49	●
8	Pilbara	Euro Basalt	Other	1	86	84	3	0.44	0.46	0.10	689	21.06	118.91	●
9	Pilbara	Euro Basalt	Other	3	245	0	0	0.00	0.00	1.00	506	21.34	119.89	●
10	Other	Winning Group	Other	1	1	1	0	0.00	1.00	0.00	132	21.71	115.17	–
11	Other	Noonkanbah Formation	Other	2	10	10	0	0.00	0.97	0.03	299	22.61	127.45	–
12	Other	Carrington Suite	Other	1	34	34	0	0.04	0.86	0.10	233	22.78	128.09	–
13	Other	Ashburton Formation	Other	1	24	0	0	0.01	0.00	0.99	221	22.83	116.11	–
14	Other	Mount McGrath Formation	Other	2	5	0	0	0.00	0.00	1.00	667	23.44	117.92	–
15	Other	Collier Group, Depositional package	Other	2	35	0	0	0.00	0.00	1.00	490	23.77	120.08	–
16	Other	Eastern Goldfields Superterrane	Greenstone	3	193	44	0	0.00	0.20	0.80	500	25.16	119.65	●
17	Other	Edmund Group, Depositional package	Other	1	65	0	0	0.00	0.00	1.00	1,172	25.25	118.52	●
18	Other	Narracoota Formation	Other	1	59	0	0	0.00	0.00	1.00	801	25.33	118.36	●
19	Other	Johnson Cairn Formation	Other	1	18	0	0	0.00	0.01	0.99	1,127	25.40	119.73	–
20	Other	Ravelstone Formation	Other	1	127	0	0	0.00	0.00	1.00	415	25.41	118.39	●
21	Other	Yilgarn Craton granites	Other	1	1	0	0	0.00	0.04	0.96	215	25.43	119.41	–
22	Other	Narracoota Formation	Other	1	23	0	0	0.00	0.00	1.00	330	25.56	119.16	–
23	Other	Millidie Creek Formation	Other	3	60	0	0	0.00	0.00	1.00	63	25.58	117.66	●
24	Other	Giles Suite 1	Intrusion	1	1	1	1	1.00	0.00	0.00	310	25.80	127.57	–
25	Narryer	Narryer Terrane metagranitic unit	Other	4	721	638	1	0.13	0.70	0.18	538	26.02	116.38	●
26	Other	Giles Suite 2	Other	1	31	31	31	0.98	0.00	0.02	222	26.06	127.84	–
27	Youanmi	Youanmi Terrane greenstones	Greenstone	1	13	1	0	0.00	0.05	0.95	152	26.33	117.73	–
28	Musgrave	Giles Suite 1	Intrusion	1	157	157	157	0.98	0.00	0.02	649	26.35	128.87	●
29	Youanmi	Meekatharra Formation	Other	1	3	3	0	0.01	0.99	0.00	49	26.64	118.56	–
30	Eastern Goldfields	Eastern Goldfields Superterrane	Greenstone	4	193	79	0	0.00	0.29	0.71	478	26.76	120.94	●
31	Eastern Goldfields	Eastern Goldfields Superterrane	Greenstone	10	292	1	0	0.00	0.00	1.00	736	26.80	121.55	●

No.	Tectonic unit	Mapped host unit (1:500 000)	Class	Bore-holes	Ultramafic m	m with X_{hyd}	Olivine-dominated m (X_{hyd} < 0.2)	Olivine	Serpentine	Talc + carb.	Max. depth	Lat. (°S)	Lon. (°E)	Fig. 3
32	Youanmi	Gnanagooragoo Igneous Complex	Other	1	81	51	0	0.00	0.51	0.49	751	26.84	117.80	●
33	Eastern Goldfields	Yilgarn Craton granites	Other	2	27	5	0	0.00	0.10	0.90	450	26.86	121.59	–
34	Youanmi	Gnanagooragoo Igneous Complex	Other	1	27	27	0	0.01	0.90	0.09	750	26.87	117.71	–
35	Youanmi	Lady Alma Igneous Complex	Other	1	18	18	0	0.01	0.88	0.11	192	26.97	118.69	–
36	Eastern Goldfields	Burtville Terrane greenstones	Greenstone	3	182	143	0	0.07	0.62	0.31	478	26.99	122.23	●
37	Youanmi	Ryansville Formation	Other	1	92	0	0	0.00	0.00	1.00	252	27.00	117.60	●
38	Youanmi	Norie Group	Other	1	19	4	0	0.00	0.14	0.86	153	27.11	118.56	–
39	Eastern Goldfields	Burtville Terrane greenstones	Greenstone	2	171	95	0	0.06	0.42	0.51	276	27.12	122.19	●
40	Eastern Goldfields	Burtville Terrane greenstones	Greenstone	1	196	95	0	0.00	0.33	0.66	270	27.17	122.19	●
41	Youanmi	Cue Tonalite	Other	1	13	0	0	0.00	0.00	1.00	435	27.42	117.91	–
42	Eastern Goldfields	Eastern Goldfields Superterrane	Greenstone	1	15	15	0	0.11	0.83	0.06	147	27.55	120.59	–
43	Eastern Goldfields	Burtville Terrane greenstones	Greenstone	2	87	8	0	0.00	0.03	0.97	249	27.62	122.35	●
44	Eastern Goldfields	Eastern Goldfields Superterrane	Greenstone	2	279	126	0	0.00	0.30	0.70	227	27.62	122.01	●
45	Eastern Goldfields	Eastern Goldfields Superterrane	Greenstone	1	76	76	40	0.61	0.33	0.06	210	27.82	120.71	●
46	Eastern Goldfields	Eastern Goldfields Superterrane	Greenstone	2	56	11	0	0.00	0.06	0.94	371	27.85	122.28	●
47	Eastern Goldfields	Eastern Goldfields Superterrane	Greenstone	2	119	0	0	0.00	0.01	0.99	502	27.95	120.50	●
48	Youanmi	Murrouli Basalt	Other	1	70	0	0	0.00	0.00	1.00	451	28.04	117.80	●
49	Eastern Goldfields	Scotty Creek Formation	Other	1	175	85	25	0.11	0.22	0.67	1,441	28.05	120.48	●
50	Eastern Goldfields	Yilgarn Craton granites	Other	1	15	0	0	0.00	0.00	1.00	381	28.07	120.98	–
51	Youanmi	Windimurra Igneous Complex, upper	Other	1	60	60	60	0.99	0.00	0.01	162	28.33	118.39	●
52	Youanmi	Big Bell Suite	Other	1	3	0	0	0.00	0.00	1.00	70	28.51	118.99	–
53	Eastern Goldfields	Yilgarn Craton granites	Other	1	23	0	0	0.00	0.00	1.00	285	28.55	122.25	–
54	Youanmi	Atley Igneous Complex	Other	1	9	0	0	0.00	0.00	1.00	116	28.58	118.90	–
55	Youanmi	Youanmi Terrane greenstones	Greenstone	1	20	0	0	0.00	0.00	1.00	146	28.69	116.41	–
56	Eastern Goldfields	Tobin Formation	Other	2	463	25	0	0.00	0.03	0.97	597	28.72	124.01	●
57	Youanmi	Youanmi Terrane greenstones	Greenstone	1	56	0	0	0.00	0.00	1.00	498	28.82	116.43	●
58	Youanmi	Youanmi Terrane greenstones	Greenstone	1	366	140	43	0.04	0.17	0.79	764	28.86	116.42	●
59	Youanmi	Youanmi Terrane greenstones	Greenstone	1	20	1	0	0.00	0.02	0.98	261	28.89	117.09	–
60	Youanmi	Yilgarn Craton metamorphic unit	Other	1	120	0	0	0.00	0.00	1.00	211	28.92	116.03	●
61	Albany–Fraser	Fraser Zone unit	Other	1	111	111	0	0.09	0.84	0.07	200	29.29	124.93	●
62	Other	Coomberdale Subgroup	Other	1	69	0	0	0.00	0.00	1.00	224	29.61	115.86	●
63	Youanmi	Yilgarn Craton metamorphic unit	Other	1	43	0	0	0.00	0.00	1.00	94	29.85	116.00	–
64	Eastern Goldfields	Burtville Terrane greenstones	Greenstone	7	2,050	1,846	591	0.40	0.39	0.21	1,469	29.93	123.21	●
65	Other	Coomberdale Subgroup	Other	1	90	0	0	0.00	0.00	1.00	98	30.08	116.08	●

No.	Tectonic unit	Mapped host unit (1:500 000)	Class	Bore-holes	Ultramafic m	m with X_{hyd}	Olivine-dominated m (X_{hyd} < 0.2)	Olivine	Serpentine	Talc + carb.	Max. depth	Lat. (°S)	Lon. (°E)	Fig. 3
66	Eastern Goldfields	Eastern Goldfields Superterrane	Greenstone	2	472	192	1	0.03	0.32	0.65	1,007	30.10	121.61	●
67	Eastern Goldfields	Eastern Goldfields Superterrane	Greenstone	1	10	0	0	0.00	0.00	1.00	83	30.16	121.27	–
68	Albany–Fraser	Fraser Range Metamorphics	Intrusion	1	310	310	0	0.13	0.82	0.05	482	30.25	124.55	●
69	Eastern Goldfields	Eastern Goldfields Superterrane	Greenstone	2	278	19	0	0.00	0.04	0.96	637	30.30	121.96	●
70	Eastern Goldfields	Eastern Goldfields Superterrane	Greenstone	5	321	9	0	0.00	0.01	0.99	451	30.35	121.28	●
71	Eastern Goldfields	Eastern Goldfields Superterrane	Greenstone	3	122	4	0	0.00	0.01	0.99	66	30.39	121.65	●
72	Eastern Goldfields	Eastern Goldfields Superterrane	Greenstone	1	11	0	0	0.00	0.00	1.00	68	30.44	121.05	–
73	Other	Paterson Formation	Other	2	77	77	0	0.17	0.79	0.04	698	30.56	123.28	●
74	Eastern Goldfields	Eastern Goldfields Superterrane	Greenstone	2	399	236	0	0.01	0.51	0.48	901	30.56	121.68	●
75	Eastern Goldfields	Eastern Goldfields Superterrane	Greenstone	1	106	13	0	0.00	0.06	0.94	249	30.56	121.51	●
76	Eastern Goldfields	Eastern Goldfields Superterrane	Greenstone	2	321	0	0	0.00	0.00	1.00	586	30.58	121.11	●
77	Youanmi	Youanmi Terrane greenstones	Greenstone	5	1,458	1,028	330	0.29	0.24	0.47	778	30.62	120.06	●
78	Eastern Goldfields	Eastern Goldfields Superterrane	Greenstone	2	13	13	0	0.00	0.69	0.31	31	30.65	121.82	–
79	Eastern Goldfields	Eastern Goldfields Superterrane	Greenstone	4	464	127	0	0.00	0.26	0.74	506	30.75	121.77	●
80	Eastern Goldfields	Eastern Goldfields Superterrane	Greenstone	6	398	0	0	0.00	0.00	1.00	1,080	30.78	121.47	●
81	Eastern Goldfields	Eastern Goldfields Superterrane	Greenstone	2	50	50	0	0.01	0.98	0.01	502	30.83	121.52	●
82	Eastern Goldfields	Eastern Goldfields Superterrane	Greenstone	4	239	0	0	0.00	0.00	1.00	587	30.91	121.71	●
83	Youanmi	Youanmi Terrane greenstones	Greenstone	4	468	6	0	0.00	0.01	0.99	403	30.98	119.12	●
84	Eastern Goldfields	Eastern Goldfields Superterrane	Greenstone	1	399	381	1	0.27	0.62	0.12	783	31.03	121.93	●
85	South West	South West Terrane greenstones	Greenstone	4	83	79	0	0.00	0.94	0.06	423	31.09	116.27	●
86	Eastern Goldfields	Yilgarn Craton granites	Other	1	4	4	0	0.16	0.80	0.04	162	31.13	121.09	–
87	Eastern Goldfields	Eastern Goldfields Superterrane	Greenstone	2	35	0	0	0.00	0.00	1.00	211	31.16	121.79	–
88	Eastern Goldfields	Eastern Goldfields Superterrane	Greenstone	12	1,030	0	0	0.00	0.00	1.00	1,009	31.22	121.69	●
89	Youanmi	Youanmi Terrane greenstones	Greenstone	2	174	173	155	0.70	0.06	0.24	366	31.28	119.33	●
90	Eastern Goldfields	Eastern Goldfields Superterrane	Greenstone	1	148	0	0	0.00	0.00	1.00	1,098	31.29	121.75	●
91	Eastern Goldfields	Eastern Goldfields Superterrane	Greenstone	5	533	13	0	0.00	0.01	0.99	320	31.30	122.60	●
92	Eastern Goldfields	Eastern Goldfields Superterrane	Greenstone	1	35	0	0	0.00	0.01	0.99	1,091	31.33	121.79	–
93	Eastern Goldfields	Eastern Goldfields Superterrane	Greenstone	4	193	163	76	0.33	0.19	0.48	675	31.38	121.49	●
94	Other	Madura Formation	Other	1	37	37	37	0.98	0.01	0.01	534	31.53	126.44	–
95	Eastern Goldfields	Eastern Goldfields Superterrane	Greenstone	1	23	0	0	0.00	0.00	1.00	149	31.59	121.97	–
96	Albany–Fraser	Fraser Range Metamorphics	Intrusion	1	26	26	19	0.89	0.11	0.01	284	31.82	123.20	–
97	Eastern Goldfields	Eastern Goldfields Superterrane	Greenstone	3	351	319	0	0.00	0.84	0.15	429	31.88	121.82	●
98	Youanmi	Youanmi Terrane greenstones	Greenstone	1	7	7	0	0.05	0.95	0.00	232	31.95	120.43	–
99	Albany–Fraser	Fraser Range Metamorphics	Intrusion	1	115	115	80	0.82	0.16	0.02	607	31.96	123.18	●

No.	Tectonic unit	Mapped host unit (1:500 000)	Class	Bore-holes	Ultramafic m	m with X_{hyd}	Olivine-dominated m (X_{hyd} < 0.2)	Olivine	Serpentine	Talc + carb.	Max. depth	Lat. (°S)	Lon. (°E)	Fig. 3
100	Eastern Goldfields	Eastern Goldfields Superterrane	Greenstone	1	96	96	31	0.52	0.41	0.07	873	32.10	121.65	●
101	Albany–Fraser	Fraser Range Metamorphics	Intrusion	1	48	48	48	0.99	0.00	0.00	325	32.23	122.90	–
102	Youanmi	Jimberlana Norite	Other	1	2	2	0	0.33	0.64	0.03	68	32.26	120.38	–
103	Youanmi	Yilgarn Craton granites	Other	2	51	50	0	0.14	0.64	0.22	128	32.43	118.18	●
104	Youanmi	Youanmi Terrane greenstones	Greenstone	1	47	47	5	0.50	0.30	0.21	161	32.59	119.74	–
105	Albany–Fraser	Biranup Zone metagranitic unit	Other	3	127	127	0	0.05	0.88	0.08	184	32.62	122.20	●
106	Youanmi	Youanmi Terrane greenstones	Greenstone	1	218	218	29	0.27	0.63	0.09	370	32.72	119.81	●
107	Albany–Fraser	Splinter Gneiss	Other	1	1	1	1	0.91	0.00	0.09	253	32.97	122.78	–
108	Youanmi	Yilgarn Craton granites	Other	1	2	2	0	0.11	0.88	0.01	99	33.14	118.60	–
109	Youanmi	Yilgarn Craton granites	Other	1	184	184	0	0.06	0.91	0.02	582	33.60	120.28	●
110	Albany–Fraser	Biranup Zone metagranitic unit	Other	1	1	1	0	0.03	0.31	0.66	70	34.54	117.19	–

Note.* Clusters with ≥ 50 ultramafic meters (●, n = 65) are drawn in **Figure 3. Coordinates are the mean borehole position of the cluster.

(b) Mapped host units and their classification, ordered by class and ultramafic meters.

Mapped host unit (1:500 000)	Class	Clusters	Boreholes	Ultramafic	Mapped host unit (1:500 000)	Class	Clusters	Boreholes	Ultramafic
Eastern Goldfields Superterrane greenstones	Greenstone	32	93	7,270	Murrouli Basalt	Other	1	1	70
Youanmi Terrane greenstones	Greenstone	11	19	2,847	Edmund Group, Depositional package 4	Other	1	1	65
Burtville Terrane greenstones	Greenstone	5	15	2,686	Millidie Creek Formation	Other	1	3	60
South West Terrane greenstones	Greenstone	1	4	83	Windimurra Igneous Complex, upper zone	Other	1	1	60
Sally Malay Suite	Intrusion	1	7	1,045	Fairfield Group	Other	1	1	44
Fraser Range Metamorphics	Intrusion	4	4	499	Madura Formation	Other	1	1	37
Panton Suite	Intrusion	1	1	235	Collier Group, Depositional package 5	Other	1	2	35
Giles Suite 1	Intrusion	2	2	158	Carrington Suite	Other	1	1	34
Millindinna Intrusion	Intrusion	1	1	157	Fitzroy Volcanics	Other	1	3	31
Narryer Terrane metagranitic unit	Other	1	4	721	Giles Suite 2	Other	1	1	31
Tobin Formation	Other	1	2	463	Ashburton Formation	Other	1	1	24
Euro Basalt	Other	2	4	331	Norie Group	Other	1	1	19
Yilgarn Craton granites	Other	8	10	307	Johnson Cairn Formation	Other	1	1	18
Scotty Creek Formation	Other	1	1	175	Lady Alma Igneous Complex	Other	1	1	18
Yilgarn Craton metamorphic unit	Other	2	2	163	Cue Tonalite	Other	1	1	13
Coomberdale Subgroup	Other	2	2	159	Noonkanbah Formation	Other	1	2	10
Biranup Zone metagranitic unit	Other	2	4	128	Atley Igneous Complex	Other	1	1	9
Ravelstone Formation	Other	1	1	127	Mount McGrath Formation	Other	1	2	5

Mapped host unit (1:500 000)	Class	Clusters	Boreholes	Ultramafic	Mapped host unit (1:500 000)	Class	Clusters	Boreholes	Ultramafic
Fraser Zone unit	Other	1	1	111	Big Bell Suite	Other	1	1	3
Gnanagooragoo Igneous Complex	Other	2	2	108	Meekatharra Formation	Other	1	1	3
Ryansville Formation	Other	1	1	92	Jimberlana Norite	Other	1	1	2
Narracoota Formation	Other	2	2	82	Marboo Formation	Other	1	2	2
Paterson Formation	Other	1	2	77	Splinter Gneiss	Other	1	1	1
King Leopold Sandstone	Other	1	2	73	Winning Group	Other	1	1	1

**Note.* 48 host units occur as the most frequent unit of at least one cluster (52 units occur among the 218 boreholes). The classification is by name only and was not adjusted for lithology. According to the unit descriptions of the 1:500 000 State interpreted bedrock geology (DEMIRS, 2018), Giles Suite 2, Jimberlana Norite and the Windimurra, Gnanagooragoo, Lady Alma and Atley Igneous Complexes are mafic or mafic–ultramafic intrusive units, and Euro Basalt, Narracoota Formation and Murrouli Basalt contain komatiitic basalt, serpentinized peridotite or mafic–ultramafic schist; all are classed as "Other" because they are not in the intrusion list and their names do not contain "greenstone". Ultramafic core mapped as Yilgarn Craton granites, Yilgarn Craton metamorphic unit or the Narryer and Biranup metagranitic units lies in bodies that are not resolved as separate units on the 1:500 000 map. The Tickalara Metamorphics borehole lies within the Sally Malay Suite cluster and therefore does not appear as a host unit here.

Table S6. Mineral state of the ultramafic core by tectonic unit, host-unit class and 5 km cluster (18,692 m, 219 records, 218 boreholes, 110 clusters). (a) Inventory and index means by tectonic unit (named as in the **Figure 1** caption) and by host-unit class (**Section S3.2**). Share is the fraction of all ultramafic meters. X_{hyd} = Srp/(Srp + Ol) is defined where Srp + Ol ≥ 0.1; its mean and the olivine-dominated fraction (X_{hyd} < 0.2) refer to the meters in which it is defined. X_{carb} = (Tlc + Cb)/(Srp + Ol + Tlc + Cb) is defined in every ultramafic meter; its mean and the talc–carbonate-dominated fraction (X_{carb} > 0.8) refer to all ultramafic meters of the group. (b) Fraction of the variance of each index (R^2) explained by the means of the groups, computed over the meters in which the index is defined; the number of groups is given because it differs between groupings and a larger number of groups favors a higher R^2.

(a) Inventory and index means.

Group	Records	Bore-holes	Boreholes ≥ 30 m	5 km clusters	Ultramafic meters	Share	Olivine-bearing meters (Ol > 0.05)	X_{hyd}			X_{carb}		
								Meters defined	Olivine-dominated meters (< 0.2)	Mean	Olivine-dominated fraction	Mean	Talc–carbonate fraction (> 0.8)
Tectonic unit													
Eastern Goldfields	114	113	76	42	10,470	56.0%	1,925	4,249	765	0.71	0.18	0.65	0.60
Youanmi	37	37	23	28	3,644	19.5%	1,340	2,022	622	0.55	0.31	0.56	0.46
Narryer	4	4	4	1	721	3.9%	343	638	1	0.86	0.00	0.20	0.13
Halls Creek	10	10	8	3	1,282	6.9%	1,279	1,281	1,276	0.01	1.00	0.01	0.00
Albany–Fraser	10	10	6	8	739	4.0%	541	739	148	0.69	0.20	0.05	0.00
Pilbara	5	5	5	3	488	2.6%	236	241	34	0.40	0.14	0.53	0.51
Musgrave	1	1	1	1	157	0.8%	157	157	157	0.00	1.00	0.02	0.00
South West	4	4	2	1	83	0.4%	0	79	0	1.00	0.00	0.06	0.05
Other	34	34	14	23	1,108	5.9%	174	356	69	0.75	0.19	0.71	0.68

Group	Records	Bore-holes	Boreholes ≥ 30 m	5 km clusters	Ultramafic meters	Share	Olivine-bearing meters (Ol > 0.05)	X_{hyd}			X_{carb}		
								Meters defined	Olivine-dominated meters (< 0.2)	Mean	Olivine-dominated fraction	Mean	Talc–carbonate fraction (> 0.8)
Host-unit class													
Intrusion	15	15	13	9	2,094	11.2%	2,025	2,093	1,612	0.17	0.77	0.02	0.00
Greenstone belt	132	131	93	49	12,886	68.9%	3,074	5,874	1,302	0.66	0.22	0.62	0.56
Other	72	72	33	52	3,712	19.9%	896	1,795	158	0.81	0.09	0.56	0.52
Total	219	218	139	110	18,692	100.0%	5,995	9,762	3,072	0.58	0.32	0.54	0.49

(b) Variance explained by group means.

Grouping	X_{hyd}				X_{carb}			
	Groups	Meters	Boreholes	R^2	Groups	Meters	Boreholes	R^2
Tectonic unit	9	9,762	126	0.37	9	18,692	218	0.22
Host-unit class	3	9,762	126	0.28	3	18,692	218	0.17
5 km cluster	75	9,762	126	0.63	110	18,692	218	0.71

Note.* Host-unit class is that of the cluster's host unit (Table S5**) and is assigned to every ultramafic meter of the cluster. X_{hyd} is defined in 9,762 m from 126 boreholes in 75 clusters; X_{carb} in all 18,692 m from 218 boreholes in 110 clusters. The tectonic-unit and 5 km-cluster R^2 of X_{carb} for the adopted criterion are the values given in **Table S2**.

Table S7. Robustness of the between-cluster and within-borehole results (**Section S4.3**). (a) Borehole-level variance partition in multi-borehole clusters: each borehole with ≥ 10 m of the index defined enters with its mean; R^2 is the fraction of the variance of these means explained by cluster means or by tectonic-unit means; the null distribution of the cluster R^2 is obtained by permuting cluster labels among the boreholes of each tectonic unit (2,000 permutations), and $p = (k + 1)/(N + 1)$ with k the permutations reaching the observed value. (b) Pooled within-borehole slopes (common slope after subtracting borehole means) on the common meters of the 34 boreholes of **Figure 2c**, and for X_{hyd} after excluding meters within 5 or 10 m of a meter that fails the ultramafic criterion, in the boreholes that still meet the selection; 95% intervals are the 2.5–97.5 percentile range of 2,000 resamples of whole boreholes or of whole clusters.

(a) Borehole-level variance partition.

Index	Meters	Bore-holes	Clusters	Units	R^2 of borehole means		SD of borehole means			Within-unit permutation null of the cluster R^2		
					Cluster	Tectonic unit	Total	Within unit	Within cluster	Median	95th percentile	p
X_{hyd}	all	47	15	6	0.89	0.69	0.38	0.21	0.12	0.78	0.85	0.0070
X_{hyd}	below 100 m	44	14	5	0.89	0.68	0.38	0.22	0.13	0.77	0.85	0.0085
X_{carb}	all	130	37	8	0.84	0.46	0.37	0.28	0.15	0.60	0.66	0.0005

Index	Meters	Bore-holes	Clusters	Units	R^2 of borehole means		SD of borehole means			Within-unit permutation null of the cluster R^2		
					Cluster	Tectonic unit	Total	Within unit	Within cluster	Median	95th percentile	*p*
X_{carb}	below 100 m	118	33	7	0.83	0.41	0.37	0.29	0.15	0.55	0.61	0.0005

(b) Pooled slopes.

Meters used	Quantity	Bore-holes	Clusters	Meters	Slope per 100 m	95% interval, resampling		Same boreholes before exclusion
						boreholes	clusters	
Common meters: X_{hyd} defined, below 100 m	X_{hyd}	34	23	6,637	−0.0378	−0.0473 to −0.0109	−0.0532 to −0.0116	–
Common meters: X_{hyd} defined, below 100 m	X_{carb}	34	23	6,637	−0.0036	−0.0217 to +0.0004	−0.0208 to +0.0004	–
Common meters: X_{hyd} defined, below 100 m	Srp	34	23	6,637	−0.0266	−0.0339 to −0.0002	−0.0336 to −0.0043	–
Common meters: X_{hyd} defined, below 100 m	Ol	34	23	6,637	+0.0360	+0.0105 to +0.0427	+0.0123 to +0.0430	–
Common meters: X_{hyd} defined, below 100 m	Tlc	34	23	6,637	−0.0005	−0.0089 to +0.0055	−0.0058 to +0.0085	–
Common meters: X_{hyd} defined, below 100 m	Cb	34	23	6,637	−0.0023	−0.0148 to +0.0001	−0.0181 to +0.0001	–
Common meters: X_{hyd} defined, below 100 m	$X_{hyd} - X_{carb}$	34	23	6,637	−0.0342	−0.0444 to +0.0011	−0.0474 to −0.0042	–
Meters within 5 m of a meter failing the criterion excluded	X_{hyd}	15	10	3,050	−0.0438	−0.0929 to −0.0106	−0.0989 to −0.0122	−0.0397
Meters within 10 m of a meter failing the criterion excluded	X_{hyd}	11	9	2,328	−0.0423	−0.1075 to −0.0061	−0.1071 to −0.0033	−0.0396

Note.* In **(a) the within-unit permutation can rearrange boreholes only in units with two or more multi-borehole clusters; for X_{hyd} these are the Eastern Goldfields Superterrane (22 boreholes, 8 clusters) and the

Youanmi Terrane (9 boreholes, 3 clusters). In **(b)** the boundary is spectral: the distance is measured to the nearest meter of the same record that fails the ultramafic criterion, not to a logged lithological contact. The pooled slope is a weighted mean of within-borehole least-squares slopes, each borehole weighted by the sum of squared deviations of its meters from its own mean depth, so boreholes logged over the longest depth ranges dominate.

Table S8. Robustness of the olivine criterion and of the host-category contrast (Section S5). Ultramafic meters, olivine-bearing meters (Ol > 0.05), talc–carbonate-dominated meters (X_{carb} > 0.8), 5 km clusters, and mapped host categories are defined as in Sections 2.1 and S3.

(a) Olivine-bearing share (%) of ultramafic meters by olivine threshold and mapped host category.

Ol threshold	All	Intrusion	Greenstone belt	Other	Intrusion / greenstone belt	Talc–carbonate-dominated meters meeting it
0.02	35.3	98.9	25.8	32.4	3.8	1.58
0.05	32.1	96.7	23.9	24.1	4.0	0.78
0.10	28.6	92.5	21.7	16.5	4.3	0.24
0.15	26.0	88.0	19.9	12.5	4.4	0.02

(b) Olivine-bearing share (%, Ol > 0.05) by weighting, with 95% intervals from resampling whole clusters within each category.

Host category	Meters	Bore-holes	Clusters	Per meter	Per borehole	Per cluster	Boreholes with ≥ 10 m olivine-bearing	Clusters with share ≥ 0.5	Talc–carbonate-dominated (X_{carb} > 0.8)
Intrusion	2,094	15	9	96.7 (87.5–100.0)	98.5 (92.7–100.0)	97.5 (92.6–100.0)	93.3	100.0	0.0
Greenstone belt	12,886	131	49	23.9 (10.0–35.1)	11.9 (5.5–20.1)	17.8 (9.6–26.5)	16.8	18.4	55.5
Other	3,712	72	52	24.1 (11.3–35.8)	20.7 (12.5–29.0)	22.3 (13.2–31.8)	20.8	21.2	52.3

(c) Leave-out tests: olivine-bearing share (%, per meter).

Host category	Test	Olivine-bearing share (%)
Intrusion	all	96.7
Intrusion	largest cluster removed (1045 m)	93.4
Intrusion	longest borehole removed (SMD157-A, 426 m)	95.9
Intrusion	any single cluster removed: min	93.4
Intrusion	any single cluster removed: max	99.9

Greenstone belt	all	23.9
Greenstone belt	largest cluster removed (2050 m)	18.5
Greenstone belt	longest borehole removed (MTD026, 1301 m)	17.3
Greenstone belt	any single cluster removed: min	18.5
Greenstone belt	any single cluster removed: max	25.9
Greenstone belt	without Eastern Goldfields	38.3
Greenstone belt	without Youanmi	18.7

(d) Spectral background: olivine weight in quartz-rich and quartz-bearing felsic meters selected without any condition on the olivine weight (serpentine + Other-MgOH + carbonate < 0.1); percentage of meters above each threshold.

Meters selected	Meters	Bore-holes	Ol > 0.02	Ol > 0.05	Ol > 0.10	Ol > 0.15	99th percentile of Ol	Maximum Ol
quartz-rich (Silica ≥ 0.7; Srp+Tlc+Cb < 0.1)	4,856	209	0.00	0.00	0.00	0.00	0.000	0.004
quartz-bearing felsic (Silica ≥ 0.3, Qz+Pl+Kfs+WhiteMica ≥ 0.7; Srp+Tlc+Cb < 0.1)	30,139	304	0.05	0.00	0.00	0.00	0.001	0.047

**Note. Host category is that of the cluster's host unit (Section S3.2, Table S5). Talc – carbonate-dominated meters meeting it (a) are the share of meters with X_{carb} > 0.8 that meet the olivine threshold. In (b) a cluster drawn more than once enters each resample as separate copies. Silica, plagioclase, K-feldspar, and white mica in (d) are the TIR (jCLST) groups of the Summary Mineral Logs; (d) describes spectral background and is not a mineralogical validation. Computed with Code/reviewer_checks.py.*